UNIVERSITAT ROVIRA i VIRGILI

Performance Study of Ammonia-Lithium Nitrate Absorption-Compression Heat Pumps for Simultaneous Heating and Cooling Applications

ABDURAHMAN HASAN ASSAGAF

MASTER THESIS

2023

Abdurahman Hasan Assagaf

Performance Study of Ammonia-Lithium Nitrate Absorption-Compression Heat Pumps for Simultaneous Heating and Cooling Applications

MASTER'S THESIS

Supervised by

Dr. Dereje Sendeku Ayou

Prof. Alberto Coronas

Master's Degree

in Energy Conversion Systems and Technologies

UNIVERSITAT
ROVIRA i VIRGILI

Tarragona, February 2023

DECLARATION

We STATE that the present master thesis, entitled "Performance Study of Ammonia-Lithium Nitrate Absorption-Compression Heat Pumps for Simultaneous Heating and Cooling Applications" by Abdurahman Hasan Assagaf, has been carried out under our supervision at the CREVER research group, Mechanical Engineering Department, Universitat Rovira i

Virgili, Tarragona (Spain)

Tarragona, February 15, 2023

Dereje S. Ayou Alberto Coronas

ACKNOWLEDGMENT

I want to begin by expressing my sincere gratitude to Allah SWT, The Almighty God, for His blessings and grace, which have enabled me to finish this master's thesis on schedule. I also give Him praise for my good health and all the advantages that made me enjoy while writing this master's thesis.

My beloved mother Fatima W. BT. M. Barakbah and my wise father Hasan Husen Assagaf, which constantly pray for their son to become a better person through this master's program, deserve recognition as well.

Prof. Alberto Coronas and Dr. Dereje Sendeku Ayou have my sincere gratitude for all of their assistance and availability throughout this work. Their advice, support, and direction have been greatly appreciated by me. I also want to express my gratitude to all the other professors who have supported me throughout my master's program.

I want to express my gratitude to all of my friends who have kept me amused and joyful throughout this study, especially Fawwaz Fauzi Mahfuzh and other friends I cannot say their names one by one here, but it doesn’t mean would decrease my gratitude to them all.

I hope that the reader will be able to understand the meaning that has been conveyed through the written words because the most important thing is the meaning, which can only be attained through the sight of logic and heart. Words are just a curtain that closes the eyes. "It is only with the heart that one can see rightly, what is essential is invisible to the eye".

ABSTRACT

A heat pump has a unique capability to provide both heating and refrigeration simultaneously. Among the work-driven heat pumping options, an absorption-compression heat pump (ACHP) system has key beneficial features including high performance and design flexibility for its deployment in industrial and non-residential building applications. In this master thesis, a double-stage absorption-compression heat pump cycle using an ammonia-$LiNO_3$ mixture as a working fluid was investigated from energy and exergy performance viewpoints. It is then compared to the same absorption-compression heat pump cycle configuration using an ammonia-water mixture, which is the conventional working fluid of the absorption-compression heat pump systems. The steady-state models of the ammonia-$LiNO_3$ and ammonia-water absorption-compression heat pump systems were developed and the heat pump's performance was simulated for a range of heating (hot water) and cooling (chilled fluid) supply temperatures of 90 °C to 105 °C and −10 °C to 10 °C, respectively. In the base-case analysis, the ammonia-$LiNO_3$ ACHP system has higher combined COP (COP_{shc}), exergy COP ($ECOP_{shc}$), and second-law efficiency ($\eta_{II,shc}$) than the ammonia-water absorption-compression heat pump system by about 23.1%, 11.7%, and 23.1%, respectively, at hot water and chilled fluid supply/return temperatures of 90/75 °C and 0/6 °C. Besides, the volumetric capacity for simultaneous heating and cooling supply was obtained as 867.9 kJ/m^3 for the ammonia/$LiNO_3$ mixture and 863 kJ/m^3 for the ammonia/water mixture. Moreover, a parametric study was also carried out for heating and cooling supply temperature ranges of 90 °C to 105 °C and −10 °C to 10 °C. The COP_{shc}, $ECOP_{shc}$, and $\eta_{II,shc}$ of the ammonia-water ACHP system were in the range of about 1.072–2.009, 0.203–0.290, and 13.7%–21.7%, respectively, for the chilled fluid supply temperature of −10 °C to 10 °C and hot water supply temperature of 90 °C to 105 °C. At the same operating condition, the volumetric capacity for simultaneous heating and cooling of the ammonia-water ACHP system was 413.7–1402 kJ/m^3. In the case of the ammonia-$LiNO_3$ ACHP system, COP_{shc} of 1.913–2.289, $ECOP_{shc}$ of 0.263–0.317, $\eta_{II,shc}$ of 23.8–24.8%, and volumetric capacity for simultaneous heating and cooling of 827.9–1352 kJ/m^3 were obtained when the hot water and chilled fluid supply temperatures are in the range of 90 °C to 100 °C and 0 °C to 10 °C.

Keywords: Absorption-compression, Heat pump, Simultaneous heating and cooling, Ammonia-water, Ammonia-$LiNO_3$, Performance comparison.

NOMENCLATURE

General:

ABS	absorber
ACHP	absorption-compression heat pump
DES	desorber
EES	engineering equation solver
EG	ethylene glycol
LCOM	low-stage compression
HACHP	hybrid absorption compression heat pump
HCOM	high-stage compression
HX	heat exchanger
MIX	mixer
SEP	separator
SEV	expansion valve
SHX	solution heat exchanger
VSHX	vapor solution heat exchanger
VCHP	vapor compression heat pump

Variables:

Δh	difference enthalpy (kJ/kg)
Δs	difference entropy (kJ/kg-K)
ΔT	temperature difference/glide (˚C/K)
Δz	difference mass fraction of strong and weak solutions (kg/kg)
ε	effectiveness (%)
η_{II}	second law efficiency (-)
$\eta_{isen,com}$	isentropic efficiency of the compressor (%)
η_m	electrical efficiency of motor (%)
η_{sp}	the pump efficiency (%)
λ_{com}	volumetric efficiency of the compressor (%)
$\dot{C}$	heat capacitance rate (kW/K)
C_P	specific heat capacity (kJ/kg-K)
COP	coefficient of performance (-)

ECOP	heat pump exergy efficiency (-)
h	specific enthalpy (kJ/kg)
$\dot{m}$	mass flow rate (kg/s)
P	pressure (bar/kPa)
pr	pressure ratio (-)
Q	vapor quality (kg/kg)
$\dot{Q}$	heat capacity/rate/duty (kW)
s	specific entropy (kJ/kg-K)
T	temperature (˚C/K)
$\bar{T}$	entropic average temperature (K)
v	suction line specific volume (m^3/kg)
VSHC	volumetric capacity for heating and cooling (kJ/m^3)
$\dot{W}$	electrical power (kW)
z	ammonia mass fraction (kg/kg)

Subscript:

abs	absorber
amb	ambient
c	cold
cf	chilled fluid
com	compressor
crit	critical
des	desorber
dif	temperature difference
el	electrical
h	hot
hcom	high-pressure stage compressor
hx	heat exchanger
hw	hot water
isen	isentropic
in	input
lcom	low-pressure stage compressor
liq	liquid

low	low
m	motor
mid	intermediate
min	minimum
max	maximum
out	out
pp	pinch point
shc	simultaneous heating and cooling
sol	solution
sp	solution pump
su	suction line
vshx	vapor solution heat exchanger
vap	vapor
vol	volumetric

LIST OF FIGURES

LIST OF TABLES

CONTENTS

1 INTRODUCTION

1.1 Background

Nowadays decarbonization and climate change issues are the problem of this generation that has been discussed frequently a few years back and has been referred to as severe issues that humanity must address (Zhu *et al.*, 2022). The industrial sector in particular is a source of problems with air quality, climate change, and other forms of pollution, and the government is constantly looking for measures to reduce greenhouse gas emissions and diminish their effects. Thereupon, long-term strategic concerns are necessary to emphasize the awareness of future planning (Worrell *et al*, 2022). Fortunately, all the people of the world now feel the same restlessness after The International Energy Agency (IEA) established our new global milestones as shown in table 1.1 to achieve the transition from fossil fuels to more sustainable and renewable sources that is necessary for the industry to reach net-zero greenhouse gas emissions by 2050 (International Energy Agency, 2022a). Energy-related and industrial processes worldwide CO_2 emissions in net zero emission are forecasted to be approximately 21 Gt CO_2 in 2030 and reach net zero in 2050.

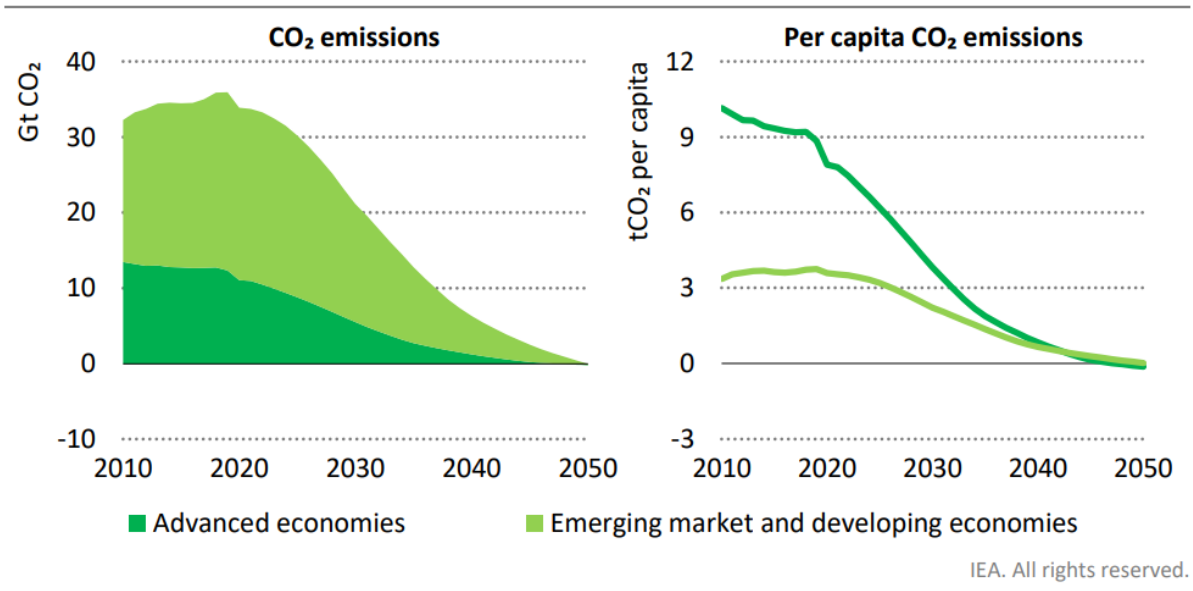

Figure 1.1. Global Net CO_2 emissions in Net Zero Emission, figure adapted from (International Energy Agency, 2022a).

As shown in figure 1.1 above explains the decrement value of carbon dioxide pollution until net zero emission can be achieved. At the end of 2045 CO_2 in advanced economies will fall to a net zero, and the emission in both emerging markets and developing economies will follow

to decrease until net zero as well before 2050. Now it can be summarized that the world is preparing globally to achieve net zero emissions in 2050.

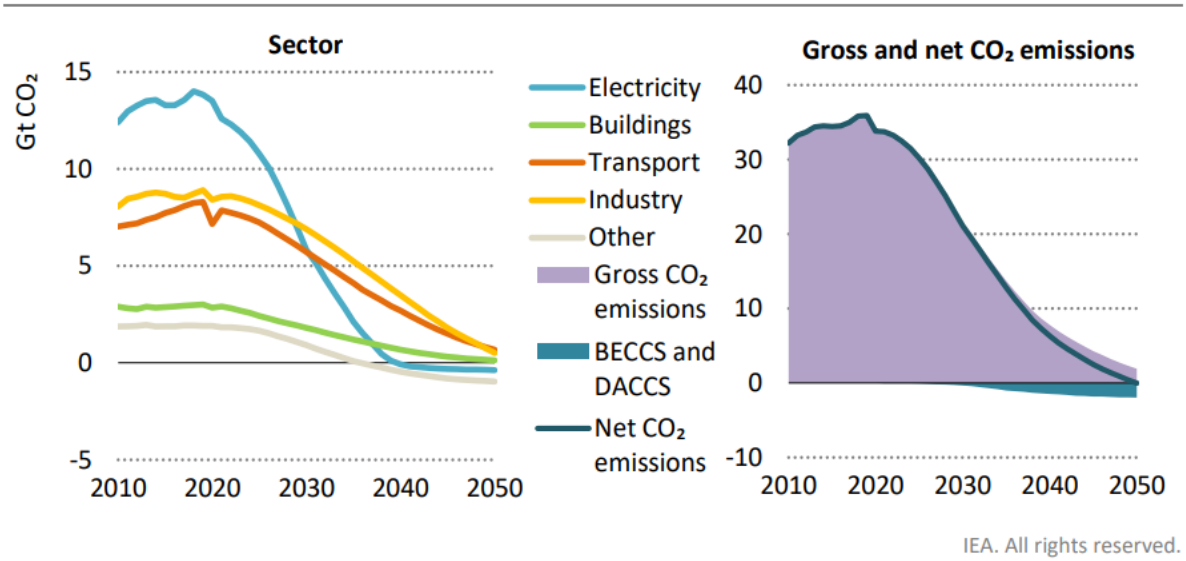

Figure 1.2. Global net-CO_2 emissions by sector and gross and net CO_2 emissions in the Net Zero Emission, figure adapted from (International Energy Agency, 2022a)

Figure 1.2 shows the forecasted emission of carbon dioxide derived by different sectors. The main factor that boosts the largest and fastest reduction in global emissions in the net zero emission is initiated by the electricity sector, which has shown in figure 1.2 above. The second greatest source of emissions in 2020 is the industrial sector, but from 2020 to 2030, it will fall by 20 % of emissions over this period while alternative methods for reducing emissions are ramped up together with the introduction of low-emissions fuels. Nevertheless, there is still a residual from the industrial sector because some areas are difficult to eliminate these emissions (International Energy Agency, 2022a).

As a consequence of that problem, heat pump technologies at the forefront of clean technologies industrial energy transition (Kim *et al.*, 2022) can be our solution to amplify the decrement and as a new resolution for eliminating the residual emission that could be produced in 2050. Another study about the bottom-up estimates of deep carbonization of U.S. manufacturing in 2050 presented that heat pump technologies are an opportunity to reduce the emission from electrification to 22 % (Worrell *et al.*, 2022).

Even though heat pump technology is not a common product that easily can be found on the market, however, as shown in figure 1.3, world energy statistic for global final energy demand

in 2019 where 19 % of total energy demand is from the industrial process heating that probably can be covered by heat pump technologies.

As has been shown in figure 1.3, the tremendous potential percentage of the demand that exists for supplying high heating temperatures at the range 100 ˚C - 200 ˚C is 27 % for industrial process heating. Therefore, there is a big potential to deeply research high-temperature heat pumps because it has already been identified that many promising applications can be utilized by this system and a bright future and clean future also will be easily achieved if there is acceleration to radically exploit more about this type of systems (International Energy Agency, 2021).

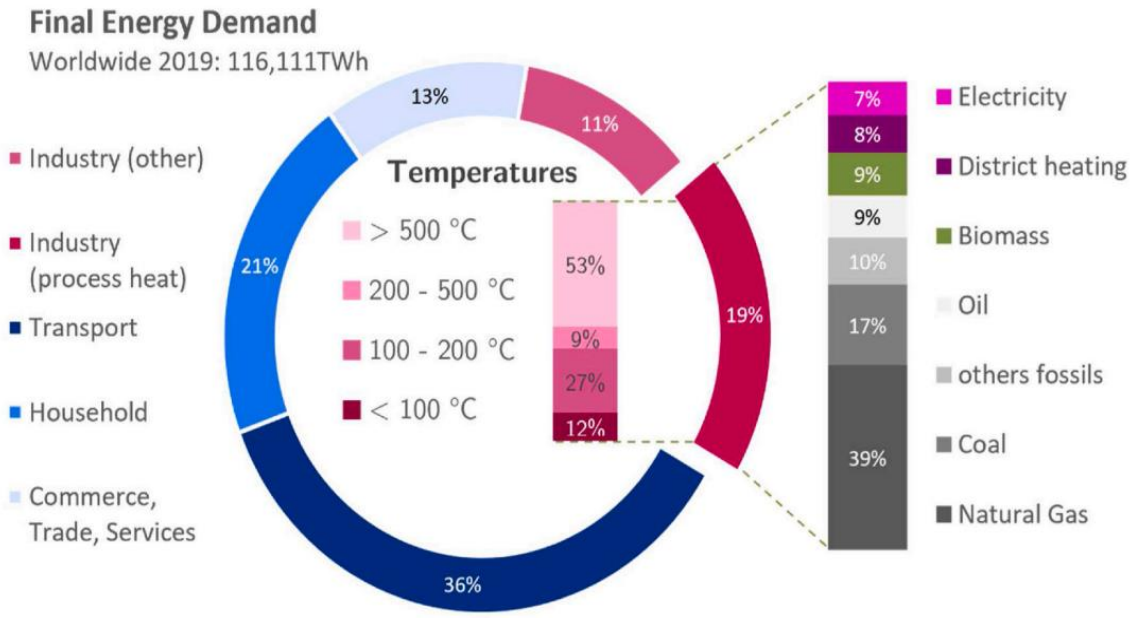

Figure 1.3. Global Final Energy Demand in 2019 by sector with estimates for application temperatures and final energy sources, figure adapted from (Adamson *et al.*, 2022)

The European heat pump market has been evaluated that can be accessible by heat pump technologies of the technical potential for 626 PJ (174 TWh) at temperatures up to 150 ˚C. From figure 1.4, the potential energy demand of 116 PJ (32.22 TWh), or 19 % of the total potential demand lies for the heating process between 100 and 150 ˚C. It might be beneficial for the food and tobacco industries and the paper industries for their chemical process. Those ranges of temperature are reachable by the high-temperature heat pump but there is a practical limitation that makes it not possible to fully exploit it with the heat pump. For the supplying temperature above 150 ˚C, the potential is bigger but still inaccessible, and need further practical research to fulfill that need.

However, if waste heat of about 100 °C is available as an input, output temperatures of up to 150 °C can already be reached. Heat pumps require special refrigerants and compressors for temperatures between 150 °C and 200 °C, but these technologies are still in the early prototype stage. Nowadays, In the paper, food, and chemical industries, industrial heat pumps are primarily used for low-temperature processes that require temperatures below 100 °C (International Energy Agency, 2022b). The complexity of industrial processes necessitates the customization of heat pumps for the applications but the promising potential demand for the heat pump pushes the researchers and manufacturers to design and customize the heat pump based on the component technologies available on the market, therefore, the potential energy demand would be exploited by this system.

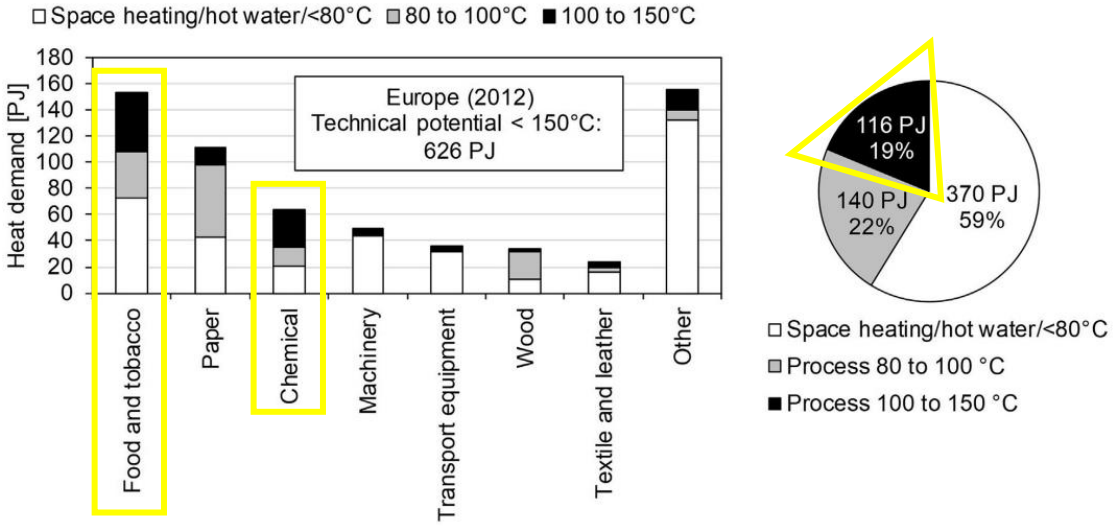

Figure 1.4. Technical market potential of process heat in Europe accessible industrial heat pumps distributed by temperature and industrial sectors, figure adapted from (Arpagaus *et al.*, 2018)

The absorption-compression heat pump cycle which the cycle is shown in figure 1.5 and several publications is also called the Osenbrück cycle because was named by the invertor that described fundamentally the basic principles of compression/absorption heat pump in 1895. It was characterized by a cycle that operated with a combination of fluids with a wide-boiling temperature between the absorbent and the refrigerant. The primary distinction between this cycle and the conventional vapour compression cycle is that the evaporation process in the desorber has not reached its full potential which created two types of phase conditions while exiting the desorber which are the liquid and the vapor conditions. Those two types of phases are separated by another component then divided into the liquid that flows to the solution pump

and is recirculated to the absorber and while the vapor proceeds to the compressor. There is also a solution heat exchanger that is used for heat recovery and to increase the energy cycle performance.

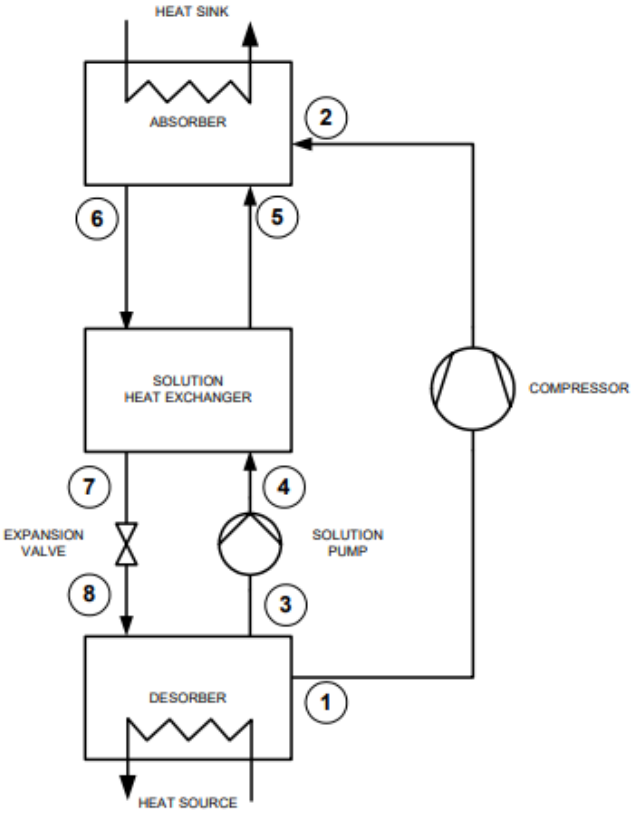

Figure 1.5. The Osenbrück Cycle, figure adapted from (Nordtvedt, 2005)

Time by time the cycle is upgraded to fulfill the needs of the civilization and industrial sectors. Consequently, the cycle that was built by Osenbrück lately is reconstructed in such a way as to improve the system. One of the most common research projects about the ACHP cycle is the idea to supply high-temperature heating and low-temperature cooling simultaneously for residential and non-residential buildings. More research pays attention to this topic because while the heat pump system wants to supply the high-temperature several restrictions and limitations must be obeyed to be able to execute that.

Jensen *et al*. (2015) investigated the impact of the rich ammonia mass fraction and circulation ratio as a feasible combination for heat sink's supply temperature at 100 ˚C, 125 ˚C, 150 ˚C, and 175 ˚C and concluded that compressor discharge temperature dominates when assessing ACHP applicability and can be reduced by two-stage cycle. Using three sets of design constraints of standard ref ($P_{high} = 28\ bar$), high-pressure NH_3 ($P_{high} = 50\ bar$), and

transcritical CO_2 ($P_{high} = 140\ bar$) allowable to supply temperatures up to 111 ˚C, 129 ˚C, and 147 ˚C while if there is no limitation of temperature discharge it can be increased up to 182 ˚C, 193 ˚C, and 223 ˚C.

Markmann *et al*. (2019) used ammonia-water as a working fluid for the absorption-compression heat pump in industrial processes. Water inlet temperatures at the heat source and heat sink are fixed at 59°C and 50°C, respectively. The poor solution mass flow rate and absorption pressure were adjusted from 0.21 kg/s to 0.31 kg/s and from 13.5 bar to 16.5 bar, respectively. At a maximum lift temperature of 43 K, the 2.5 of maximum COP for supplying a heating power of more than 40 kW can be attained and given.

Gao *et al*. (2020) developed two novel approaches of an absorption-compression heat pump with two-stage rectification to reduce the suction temperature of the compressor and lower its temperature discharge and by utilizing a subcooler proposed to reduce the irreversible loss during the throttling process, the heat pump now has better energy efficiency.

Qing *et al*. (2021) simulated about three types of ACHP cycles (heat recovery, liquid injection, and flash tank cooler) with a temperature lift of 40K at $P_{high} = 50\ bar$ and obtained that single-stage ACHP cycle cannot meet the requirement while those three types of two-stage cycle easily achieve that, especially while using the flash tank cooler can achieve the temperature lift until 50K.

Ayou *et al*. (2022) evaluated the performance of a two-stage absorption-compression heat pump for simultaneous heating and cooling with the temperature at 100 – 150 ˚C and -10 – 10 ˚C found that the combined heating and cooling COP of about 2.02 – 4.04 and the exergy efficiency of 0.467 – 0.483 can be achieved with technical constraints of the R717 compressor technology that available in the market (compressor discharge temperature ≤ 190 ℃).

Many studies have been published to examine the benefits that heat pump technology can offer for providing cooling in addition to heating while also being used in industrial and non-residential applications. Ayou *et al*. (2022) studied an ammonia-based compression heat pump to deliver heating (65–95 ˚C) and cooling (2 ˚C) simultaneously for milk pasteurization processes. Nordtvedt *et al*. (2011) designed a hybrid heat pump for waste heat recovery for the food industry in Norwegia with the heat sink supply temperature up to 100 ˚C and recovering waste heat at approximately 50 ˚C. According to the energy analysis of solar energy or waste heat recovery accounts for 33.0% of all energy sources in the new dairy, and the process has a

waste heat recovery rate of over 95% (Ahrens *et al.*, 2021) when the system was investigated for a green field dairy in Norway to provide heating and cooling simultaneously.

1.2 Motivation

Heat pump systems provide affordable options for recovering waste heat from numerous sources for use in various industrial, commercial, and residential applications. One of the most workable solutions to the greenhouse impact is provided by heat pumps. It is the only procedure that is currently known to recycle waste heat and environmental heat back into a heat production process, providing environmentally friendly and energy-efficient heating and cooling in applications ranging from residential and commercial buildings to process industries (Chua et al., 2010).

The main advantage of this system is the waste heat that is produced in the industry is recovered from every possible source of waste heat and turn it into a useful output that can improve the energy efficiency of many industrial operations. Commercial heat pumps have many uses in a range of industries since they are based on the vapor compression cycle or the absorption compression cycle.

Over the vapor compression cycle, the absorption-compression cycle demonstrated two key benefits. The benefit was the ability to regulate a wide range of capacities due to simple adjustments of the mixture composition. The second was the temperature glide in the absorber and the desorber, which resulted in a significantly greater heating coefficient of performance (Bergland, 2011).

A multi-stage heat pump is a system that works with more than one compression stage, and it also can be classified as a compound or cascade system. The compound systems consist of two or more compression stages which are the high-stage compressor and the lower-stage compressor that is connected in a series. Normally it also consists of three types of pressure that work to elevate the pressure inside the system which are high pressure, intermediate pressure, and low pressure.

A multistage system provides more flexibility, greater compression ratio, higher compression efficiency, and refrigeration effect compared to a single-stage system (Agrawal *et al*, 2007). The other important thing is it also has a lower discharge temperature at the high-stage compressor because the compressor technologies are limited the temperature at a certain

condition. Based on research into the ammonia compressor technology currently in use, the compressor discharge temperature limit was determined to be 190 C (Bamigbetan *et al.*, 2017).

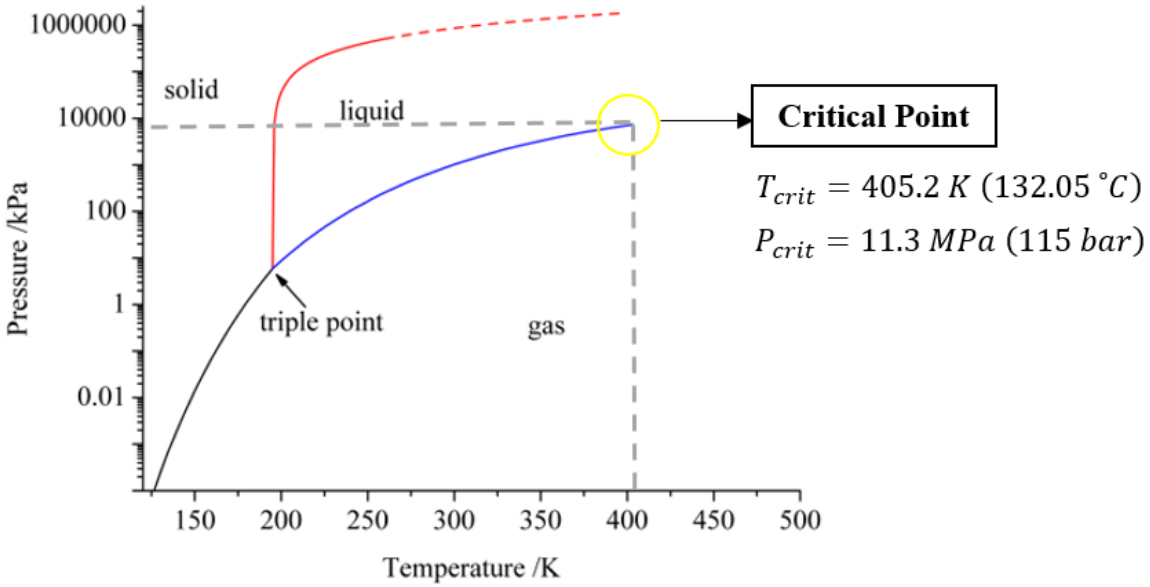

Figure 1.6. Pressure-temperature phase diagram of ammonia, figure adapted from (Richter *et al*, 2014)

Absorption-compression heat pump cycle normally is carried out by a zeotropic mixture in which the boiling temperature of both fluids is different, and it's decided the composition of the components and pressure while on the other hand the azeotropic it's very rigid because the boiling temperature is constant and dependent on the pressure.

Supposing it works with only a single fluid like the one that is common in the market which is ammonia, it is also limited by the temperature and the pressure of it, therefore the system cannot lift the working fluid to the high temperature because it is limited by the critical point that makes supplying the high temperature in the heat sink is hard to achieve.

As appears in figure 1.6, there is a point of the pressure and the temperature ($T_{crit} = 405.2\ K\ (132.05\ ^{\circ}C)$ and $P_{crit} = 11.3\ MPa\ (115\ bar)$ which is the *critical point*. The concept is when it works above the critical point it cannot be liquefied regardless of the applied pressure (Kobe et al., 1952). Above the critical point, no line separates the compressed liquid region and the superheated vapor region (Cengel et al, 2015). It is challenging to liquefy the vapor in this scenario if the working fluid works over its critical temperature, regardless of how

many different pressure values are applied. It is therefore difficult to design a system that can deliver a high temperature using only one liquid.

The combination of ammonia with another fluid probably will increase the critical point. It depends on how much the mass fraction or mole fraction is while mixing those two mixtures. For the ammonia and water mixture data as shown in table 1.1, H Rlzvl *et al*. (1987) investigated the critical point of ammonia – water combination and acquired that the more water was added to the combination, it will increase the critical temperature of the mixture. Therefore, using ammonia–water mixture will able to make the system performs at a higher temperature which also increases the chance to supply high temperature.

Table 1.1. Ammonia-water critical points (H Rlzvl et al., 1987)

Mole fraction (NH_3)	**Temperature, (K)**	**Pressure, (kPa)**
/0.166	618.1	22.37
0.224	610.2	22.52
0.387	579.7	22.39
0.570	526.2	21.42
0.748	483.3	19.00
0.870	451.5	16.05
0.936	422.5	13.85
0.972	411.9	12.47
1.000	405.5	11.15

Since the condensing pressure drops for an ammonia/water mixture, using a zeotropic fluid allows for higher temperatures than ammonia-based vapor compression heat pumps. Besides that, Nordtvedt (2005) concluded that using a zeotropic mixture can be more convenient than a single liquid because of the flexibility to adjust the capacity control in the cycle. The non-zeotropic fluid can also be adjusted but only by changing the pressure and the mass flow rather, whereas the zeotropic mixtures have more flexibility to adjust the system by the ammonia concentration in the absorber and the desorber. As shown in figure 1.6, the reduction of ammonia mass fraction also will reduce the temperature at constant pressure. When the ratio of ammonia concentration is changing consequently the capacity will follow.

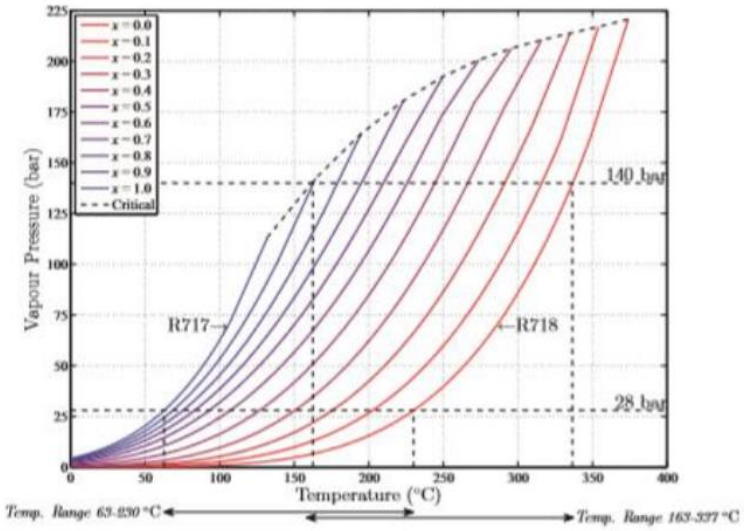

Figure 1.7. Vapor pressure, temperature, concentration diagram for ammonia–water, figure adapted from (Bjørvik, 2019)

Nordtvedt, (2005) also mentioned that because the components of the mixture that haven't evaporated are changing in the desorber, which results in a different boiling point through the process, the phase changes in the desorber and absorber are non-isothermal. As a result, the losses in the heat exchangers will be reduced, and the system's coefficient of performance (COP) will rise if the temperature glide in the absorber and desorber matches the temperature glide in the heat sink and heat sources.

Zühlsdorf et al. 2018) showed raising the temperature of ultra-low temperature district heating to 60 C using a booster heat pump utilizing the specified mixed working fluids is an efficient, viable, and long-lasting solution.

1.3 General Objective and Specific Objective

This idea of the investigation is to compare the zeotropic mixture that is well-known in the market, which is ammonia-water with ammonia-lithium nitrate. The purpose is to supply cooling and heating temperatures simultaneously for non-residential building applications. The main objective of this master thesis project is to evaluate the performance of ammonia/$LiNO_3$ absorption/compression heat pumps (ACHPs) for simultaneous refrigeration (−10–+10 °C) and heating (≥90 °C) applications, and then performance comparison with the ammonia/water ACHPs for identical operating conditions. In addition, it also does a parametric study and evaluates it after the effects that influence the key operating conditions and design variables on

the system performances. Engineering Equation Solver (EES) software will be used in this study's numerical modeling to evaluate performance, and the results will be discussed.

1.4 Justification

From the background research of this master thesis, several data and graphs are shown to make sure that the potential energy demand of heating and cooling in the industry is high and the door for the heat pump technologies to compete as equipment to supply heating and refrigerating in the industry still wide open. Nonetheless, the development of the technologies and the research cannot be complied their needs because of the complexity of the industrial needs. Supply at a high temperature for industrial applications still needs to be improved and tailored to the higher level of technology readiness (International Energy Agency, 2022b). Accordingly, the research about the heat pump to supply cooling and high-temperature heating simultaneously could be interesting and beneficial. However, the cooling and heating supply from the double-stage absorption-compression heat pump system is limited (Wu et al., 2018a; Ayou et al, 2022), and plentiful paper is only research for high heating temperature heat pumps (Kim *et al.*, 2013; Jensen *et al.*, 2015; Liu *et al.*, 2018, 2019). Moreover, the application of ammonia-lithium nitrate as the working fluid not yet has been investigated. Therefore, it is interesting to investigate the performance of ammonia-lithium nitrate and compare it with the ammonia-water to know the output of the system using the new zeotropic mixture as a new reference for the heat pump. Consequently, in the future, the option to develop a heat pump for cooling and heating purpose might be heading in various directions. Even more, the main purpose of this research is to contribute as a particular solution to our global challenge to reduce the CO_2 impact of abusive consumption in the cooling and heating sectors of non-residential buildings.

This master thesis includes the knowledge of the subject Determination of Thermodynamic and Transport Properties of Fluids (Salavera., 2021) to calculate the vapor and liquid mixtures of the ammonia-lithium nitrate, Advanced Thermodynamic Engineering and Thermal Conversion Energy Technologies (Coronas., 2021, 2022) to model each component and the system of the double-stage absorption-compression system.

1.5 Methodological Approach Followed and Thesis Structure

There are five chapters for this master thesis. Chapter 1 is an introduction to explain and describe what is the background, motivation, objectives, and justification of this research.

Chapter 2 is an explanation of the heat pump systems and components description while it included the schematic diagram of the system and a detailed description of the compressor technologies. Chapter 3 shows a modeling methodology that is contained modeling assumptions, a model of each component, thermodynamical properties of liquid and mixtures that are used in the system, performance indicators of the system, and model validation. Chapter 4 delivers the simulation result and discussion about the comparative study between ammonia/water and ammonia/$LiNO_3$ and the parametric study to know the effect of key operating conditions and design variables on the system. Chapter 5 is conclusions from the result and the analysis of this research.

2. HEAT PUMP SYSTEMS AND COMPONENT DESCRIPTION

2.1 Description of Two-Stage Absorption Compression Heat Pump Cycle

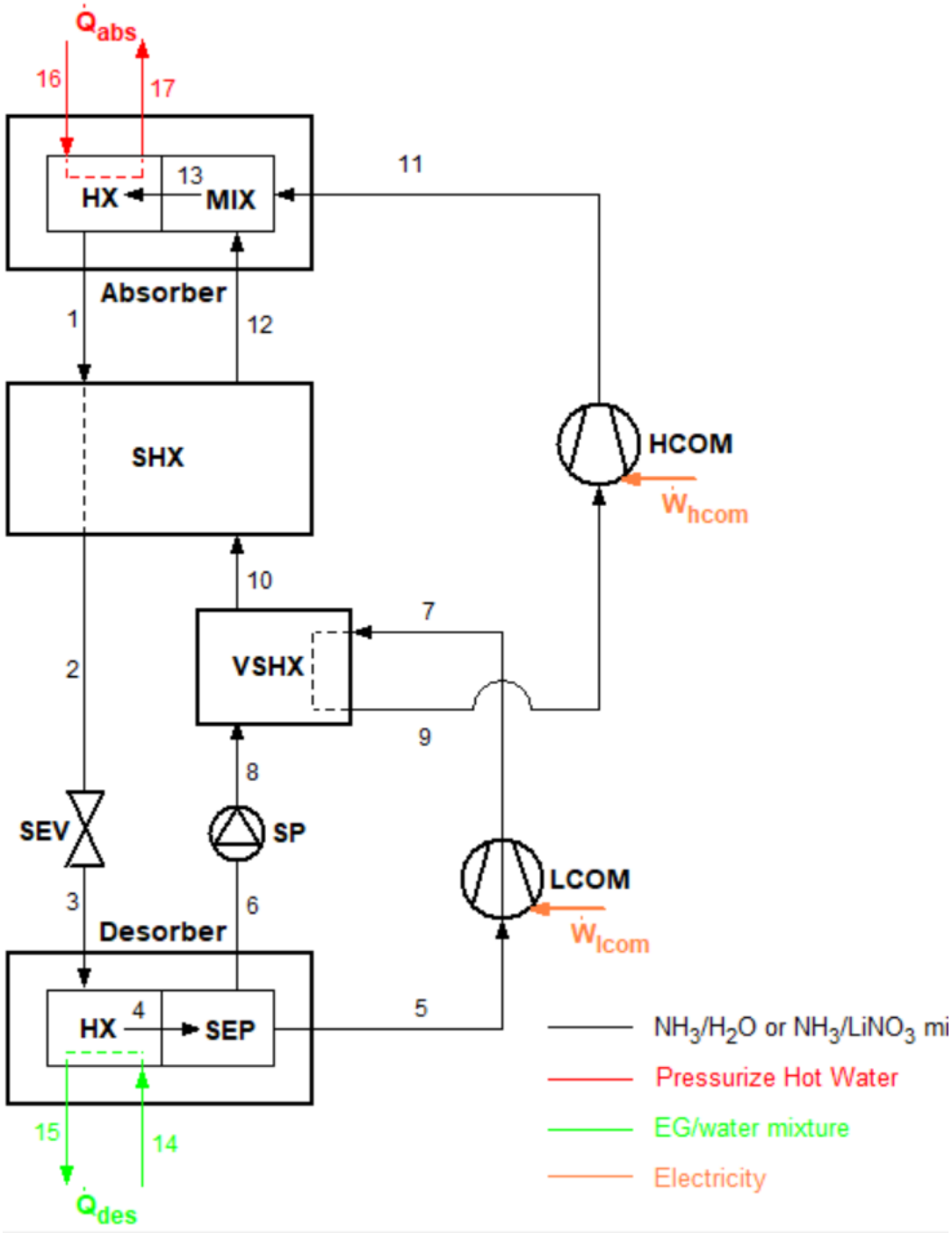

Figure 2.1. Schematic diagram of two-stage absorption-compression cycle

This heat pump system that has been used in the cycle is double-stage absorption-compression heat pump using two types of zeotropic working fluids as has been discussed before. Two types of zeotropic working fluids are going to be simulated with this schematic diagram, the first one

is the one that is commonly used in the market of heat pump systems which is the combination of ammonia – water as a mixture, and the second one is ammonia – lithium nitrate. These two zeotropic working fluids are going to operate at the same schematic diagram and the same working and operating conditions to achieve the same temperature gliding and lift for simultaneous heating and cooling in heat pumps.

Above is the schematic diagram of absorption–compression heat pumps shown in figure 2.1. The components of the ACHP cycle are an absorber and desorber, an expansion valve (SEV), two dry compressors (low compressor, LCOM, and high compressor, HCOM), and a solution pump (SP), a solution heat exchanger (SHX), a vapor solution heat exchanger (VSHX), a liquid–vapor separator (SEP), a vapor–liquid mixer (MIX). This ACHP cycle is designed for two types of purposes to give simultaneous heating and cooling at the same time (stream 16 → 17 and stream 14 → 15). This system was already adjusted to work with the high temperature and pressure, consequently, it needed more than one compressor to achieve the high-temperature lift between the heating supply and cooling supply. Two types of heat exchangers are designed to build an effective system since the temperature leaving the low compressor is too high and can be useful to transfer that heat to the weak solution. The main reason is the system is also limited by the temperature discharge of the compressor technology and it will be discussed further in the next subchapter.

2.2 Description of Heat Pump Cycle and Its Components

As we can see in the ACHP cycle that showed in figure 2.1. that cycle is purposed to supply the high temperature and the cold temperature at the same time, fundamentally, for that reason there are some parts of the model that required concentration while designing it. Especially the compressor because the technology is limited by the maximum temperature discharge and the other side is also limited by the value of the liquid that can be entered through the suction of the compressor. Besides that, there are a lot of design constraints that must be included while designing this system. This subchapter explains how each component works synchronously to deliver the cold temperature below 0 ˚C while operating at the high-temperature lift and provide a hot temperature above 90 ˚C and those temperatures must be supplied simultaneously.

2.2.1 Ammonia-water mixture as a working fluid

The ACHP cycle is designed to supply the heating temperature (stream 16 → 17) and cooling temperature (14 → 15) which can be useful for several processing industries. First, the cycle

begins from stream 1 while the temperature is adjusted with the temperature difference of inlet external stream 16, and the same approach is also done to know the temperature at stream 6. The temperature is lowering (stream 1 → 2) because the strong solution is transferred the heat while passing the SHX to the weak ammonia solution (stream 10 → 12). The idea of transferring the heat is because it can be useful as a preheat for the weak ammonia solution before entering the absorber. In consequence, there is another preheat also featured in the system by vapor-solution heat exchanger VSHX with not only works with the same approximate purpose to preheat (stream 8 → 10) but that component is also added to lowering the temperature before entering the high compressor (7 → 9) because is limited with the temperature discharge and will be discussed further. The Strong ammonia–water solution temperature and pressure condition are lower down (stream 2 → 3) after leaving the SEV to be able to absorb more heat from the heat source before entering the desorber. After gaining heat at the desorber, consequently, now two types of phases leave the desorber and are separated at SEP (stream 4 → stream 5 and stream 6). The highly pure ammonia vapor transforms into a high-temperature and high-pressure (stream 5 → 6) as it enters the LCOM. On the other side, the liquid form of the weak ammonia solution is pumped up by the solution pump (SP) increased the pressure, and is ready to pass through the VSHX (stream 6 → 8). When the preheating process for the weak ammonia solution occurred in VSHX and SHX (stream 8 → 10 and stream 10 → 12), besides the temperature discharge, one must be paying attention also to the vapor before entering the HCOM (stream 9) because there is a consideration of the amount of vapor that allowed to enter the dry compressor. Because of the heat transfer that occurred in the VSHX, the temperature and pressure of the vapor solution after leaving VSHX must be increased once again to achieve our demand of the high value of heating supply above 90 ˚C on the desorber. By passing through the second compression in HCOM (stream 9 → 11) now the compressed high temperature is ready to be combined with the ammonia–water weak solution on the MIX (stream 11 + 12 → 13) and then enters the absorber. At this time, the ammonia vapor is absorbed and turned into a solution after leaving the absorber because the heat is transferred to the external stream and increases the temperature in it.

2.2.2 Ammonia-lithium nitrate mixtures as a working fluid

A similar process also occurred while calculating the model of ammonia-lithium nitrate, but the difference is that the ammonia-lithium nitrate has a large temperature boiling point, therefore, no amount of lithium nitrate vapor will be generated and entered the compressor.

The compressor only works with single fluid ammonia unlike the ammonia-water as a working mixture because there is a high possibility of water can be created and entered the compressor. That is the reason why the compressor for the ammonia-water system has a regulation of water vapor limit to enter there.

The ACHP cycle is designed for the same purpose as ammonia-water and the process is also more or less the same, the main difference the compressor only works for single-fluid ammonia. The system also supplies the heating temperature (stream 16 → 17) and cooling temperature (14 → 15). First, the cycle begins from stream 1 with the high-pressure condition and gets the amount of mass fraction, the temperature is adjusted with the temperature difference of inlet external stream 16, and the same approach is also done to know the temperature at stream 4. The temperature at state 4 is the same as state 5 and state 6 because of the assumption of the equilibrium system, therefore, by inputting the difference max fraction the low pressure can be obtained. In consequence, because the high pressure is already obtained, the work of the pump also can be calculated and properties at state 8 can be gained. The ammonia vapor stream state also can be acquired easily by two other properties. The work of compressor and heat VSHX also can be obtained by assuming the vapor quality leaving LCOM is 1.

The other difference is to obtain the properties of vapor-liquid ammonia solution need to be calculated by the property of vapor ammonia and the liquid of the lithium nitrate as each state and doing mass balance for the mixture to know the amount of vapor that generated at the two-phase conditions.

For the general mass balance of the system, there is no mass fraction of the lithium nitrate, which means the compressor only works with single fluid ammonia, the mass balance can be calculated easily because the mass fraction is equal to 1 ($z_5 = 1$).

Each of the main components has a different type of job of the working process and procedure to be able to work synchronously and achieve the high and cold temperature supply simultaneously. For that reason, below is the explanation detailed working mission of each component that is designed in the schematic diagram.

2.2.3 Absorption – Desorption heat pump process

The ACHP cycle is based on the Osenbruck cycle, but in the case of heat pumps some processes like evaporation and condensation are substituted by desorption and absorption while it uses zeotropic mixtures with a wide boiling temperature as the working fluid mixture.

The absorber is one of the HACHP system's most important components and the absorber pressure has a greater impact on the capacity of the absorber than the concentration of the ammonia weak solution (Jung et al., 2014).

While passing through the desorber (stream 3), the zeotropic fluid is getting some value of heat by an external heat source (stream 14 → 15). Usually, that source is getting from the heat that no longer wanted to be used again in the chemical industry. After increasing its temperature, the zeotropic fluid is evaporated in the desorber using heat transfer from the heat source (Nordtvedt *et al.*, 2011), and it became two phases of a mixture at the end of the desorber. The first one is the high vapor mixture (stream 5 → 7 → 9 → 11) where typically it is ammonia because the ammonia and water combination are the most typical refrigerant pair for absorption–compression hybrid cycles (Adamson *et al.*, 2022). The second one is the weak solution in form of liquid (stream 6 → 8 → 10 → 12). Those two-phase mixtures are separated in thermal equilibrium and divided into saturated liquid and saturated vapor. In the real case, a phase separator is needed to separate the ammonia vapor from the solution leaving the desorber since complete evaporation does not occur in the desorber (Ahrens *et al*, 2019b).

The vapor and the weak solution will be mixed again before entering the absorber (stream 11 and stream 12). The vapor and liquid phases are combined before entering the absorber using an adiabatic process (stream 13), creating a vapor–liquid combination in thermal, mechanical, and chemical equilibrium (Jensen *et al.*, 2015). At this moment, the absorption phenomenon takes place by cooling down the temperature of the internal stream in the desorber and transferring it to the heat sink (stream 16 → 17). This process takes a place at both external and internal temperatures and because of that mixing process, the fluid now becomes the rich solution again at the end of the absorber (stream 1).

2.2.4 Compressor Technologies

The compressor works in this ACHP system by compressing and elevating from low pressure to the high-pressure condition of the vapor solution that is already separated from the liquid weak solution (stream 5 → 7 and stream 9 → 11).

In case to achieve the high-temperature lift for simultaneously supplying low-temperature and high-temperature at the same time, selecting the compressor technologies is one of the most important aspects to develop the ACHP system. For achieving the high-temperature lift is tremendously needed compressor technologies that can help to elevate the temperature and pressure. Therefore, several constraints limit while designing a compressor model for the ACHP system to increase those properties.

Neksfit *et al*. (1998) studied CO_2 heat pumps to supply temperatures above 90 ˚C concluded that up to 180 °C discharge temperatures ought to be manageable with standard lubricants. Ahrens *et al*. (2019a) stated that to get a high-temperature lift, a discharge temperature of at least 180 °C must be tolerated by the compressor. Ommen *et al*. (2014) researched about two compressor technologies, the maximum pressure for the low-pressure ammonia compressor (LP R717) is 28 bar and 180 C is the maximum discharge temperature allowed. The high-pressure ammonia compressor (HP R717) can withstand discharge temperatures of up to 180 C and a maximum pressure of 50 bar. Bamigbetan *et al*. (2017) Also studied the limitation of the compressor discharge temperature based on the current ammonia compressor technology and found that 190 ˚C is the value of its limit.

Besides the temperature discharge, there is another thing that must be considered which is the amount of water content that is allowable to enter the compressor. The vapor solution should be avoided having water content higher than 5 %, otherwise, the system is infeasible (Jensen *et al.*, 2015). In the other study, Nordtvedt (2005), modeled with Sabroe TCMO compressor, and based on discussion with the compressor manufacturer and lubricant oil manufacturer, 2.5 weight-% and 160 ˚C are used for the maximum allowable water content and the maximum discharge temperature.

Table 2.1. Compressor Technologies from Manufactures.

Manufacturers	Model	Maximum Condensation Temperature	Maximum Pressure Discharge	Design Suction Pressure	Design Differential Pressure	Maximum Temperature Discharge
GEA	Grasso L XHP	95 ˚C	70 bar	NA	NA	140 ˚C
GEA	Grasso V XHP	+ 95 ˚C	63 bar	30 bar	50 bar	NA
Johnson Controls	HPX	+ 90 ˚C	60 bar	26 bar	40 bar	NA
Mayekawa	HS	90 ˚C	60 bar	NA	NA	NA

The suction pressure and the maximum pressure discharge are the other aspects which are needed to consider. Each manufacturer has its limited number of suction pressure and maximum pressure discharge. Here below are several data from different manufacturers of ammonia high-temperature compressors for supplying heating more than 90 ˚C.

When choosing compressor technologies, two types of aspects need to be considered first, which are isentropic efficiency and volumetric efficiency. By those two efficiencies, the compressor characteristic also can be described. While the isentropic efficiency is also considered the main influence of the compressor temperature discharge (Jansen et al, 2015). Normally, there is some polynomial function fitted to the data that provided by manufacturers to obtain isentropic efficiency and volumetric efficiency (Nordverdt et al, 2005).

The polynomial form of the isentropic efficiency is as follows:

$$\eta_{isen} = C_0 + C_1 \cdot pr \tag{2.1}$$

The equation for volumetric efficiency is:

$$\eta_{vol} = C_0 + C_1 \cdot pr \tag{2.2}$$

C_0 and C_1 calculated by the least squares approach of fitting data supplied by the compressor manufacturer. Those values of C_0 and C_1 change following what type of compressor it uses and the performance characteristic that it has. Here below in table 2.2 the several isentropic efficiency and volumetric efficiency from the several journals that have already been collected.

Table 2.2. Compressor Technologies from Journals

Authors	Isentropic Efficiency	Volumetric Efficiency	Max Temperature Discharge
Bergland (2011)	$\eta_i = 0.9051 - 0.0422pr$	$\eta_v = 1.0539 - 0.0788pr$	170 ˚C
Wersland et al., (2017)	$\eta_i = 0.3862 + 0.0016\pi^3 - 0.0333\pi^2 + 0.1892\pi$	$V_S = \frac{\dot{m}_{comp} v_{comp}}{\lambda n}$ $\dot{m}_{1st\ comp} = 0.022\ m_3$ $\dot{m}_{2nd\ comp} = 0.00185\ m_3$	160 – 170 ˚C
Wu et al. (2018b)	$\eta_i = 0.976695 - 0.0366432pr + 0.0013378pr^2$	$\eta_v = 0.994 - 0.885(pr\frac{1}{k} - 1)$	-
Wersland et al. (2018)	$\eta_{i,pis} = 0.7876 - 0.0006\pi$ $\eta_{i,screw} = -0.00004 * \pi^4 - 0.0222 * \pi^3 - 0.0419 * \pi^2 + 0.0419 * \pi - 0.1783$	$\eta_{v,pis} = 1.0056 - 0.0374\pi$ $\eta_{v,screw} = 0.95 - 0.0125\pi$	190 ˚C
Liu et al. (2019)	$\eta_i = -0.00097\pi^2 - 0.01026\pi + 0.83955$		180 ˚C
Bjørvik (2019)	$\eta_{i,rec} = 0.9051 - 0.0422 \cdot pr$ $\eta_{i,screw} = 0.9051 - 0.0222 \cdot pr$	$\eta_v = 1.0539 - 0.0788 \cdot pr$	170 ˚C

Bergland (2011) investigated four scenarios with different temperature discharge limitations with the equation that (Nordtvedt, 2005) got from the manufacturer's data, and found that at the maximum temperature discharge of 150 ˚C, the COP value is 3.85 and at the maximum temperature discharge of 250 ˚C the COP value is 2.08. With the same equation (Bjørvik, 2019) found a COP of 3.677 and an outlet sink temperature of 98 ˚C, the compressor discharge temperature in the simulation is 180 ˚C with an injection ratio of 0.053. The variation of mass flow from 10 % to 130% of the heat sink has been done and the value of temperature discharge is still in the allowable range (Wersland *et al*., 2017). While with the isentropic efficiency and volumetric efficiency equation, Wu et al., (2018b) studied that the heat pump using two cycles (single effect and generator-absorber heat exchange) can realize more flexible capacity ratios for hot, mild, and cold conditions than single-effect cycle. The other research from (Wersland *et al*., 2018) showed that utilizing two – stage piston compressor can be able to supply a temperature of 115 ˚C by optimizing the intermediate pressure obtained 2.04 COP with the circulation ratio 0.72 at 190 ˚C maximum temperature discharge, otherwise, the screw compressor had a lower performance. Liu *et al*. (2019) The study revealed that using an ammonia-rich solution mass fraction less than 0.6 and a circulation ratio greater than 0.7 is a wonderful choice for the hybrid ACHP system in actual application to gain superior thermal performance while the discharge constraint is 180 ˚C.

After temperature discharge, the second highest influence is from the absorber pinch point temperature difference followed by the desorber temperature difference. Both increase the compressor discharge temperature due to the increased pressure ratio over the compressor (Jensen *et al.*, 2015). The pinch point is the area of the heat exchanger where the temperature differences between the heat-exchanging mediums are the lowest. For ammonia-water combinations with a high ammonia content, the pinch point in the absorber is somewhere in the center of the heat exchange, on the other side the desorber's pinch point is at the input or exit of the heat exchanger (Nordtvedt, 2005). The pinch is generally easy to spot on a heat exchanger diagram. The pinch point typically, but not always, appears near the heat exchanger's intake or exit. A pinch point suggests that the heat exchanger design may benefit from upgrading. The pinch point serves as a bottleneck for the energy transfer if the two traces on the heat exchanger diagram are not nearly parallel (Herold *et al*., 2016).

As it showed on the schematic diagram because it’s not practical to set the value of the pinch point at the middle of the heat exchanger whether the value of the pinch itself, therefore, there

is some practical approach that only sets the value of temperature difference between an internal stream and the external streams on the absorber (state 1 and state 16) and the desorber (state 4 and state 14) but must also take into the consideration of the pinch value at the same time that while inserting the value of the temperature difference on those states.

Must consider also the sub-atmospheric issue of the operating condition of the heat pump systems because it must be above the atmospheric pressure ($P_{low} = 1\ bar$) to prevent air entrainment in the system (Jensen *et al.*, 2015).

3 MODELLING METHODOLOGY

This section shows some general assumptions, the process of modeling the components of a two-stage ACHP system with the relevant manufacturer's data to do the comparative study about the zeotropic mixture that easily can be found on the market, which is ammonia–water mixtures, and then compares it with another zeotropic mixture of ammonia – lithium nitrate.

To simulate the double-stage absorption-compression system, the same input and assumption will be used and at the end, both performances will be compared. In this case, to build the system of the absorption-compression heat pump, several limitations need to be considered and all the limitation of the system has been discussed also in chapter 2.

This chapter will be more focused on developing the calculation of each component, all of them will be calculated thermodynamically using several equations to define the properties of each state point. The ACHP model has developed steady-state operation and the heat pump also can operate in dynamic or transient. The modeling of the heat pump is acceptable simplifying, several assumptions are considered for this heat pump system to reduce the complexity of calculating the whole system.

The commercial software of Engineering Equation Solver (EES) will be used to carry out steady-state simulation of the heat pump system, which is widely used in heat pump process simulation (Jensen *et al.*, 2014; Ally, Sharma and Abdelaziz, 2017; Salehi and Yari, 2019). The properties of ammonia – water mixture are obtained from EES from the correlation (Ibrahim and Klein, 1993), while the properties of the ammonia–lithium nitrate is calculated using the correlation obtained based on the experimental data of ammonia–lithium nitrate (Salavera *et al*., 2018) upgrading the scarce of the experimental data from the previous research (Libotean *et al.*, 2007, 2008).

Finally, the result of each model will be compared in two ways, at the defined base case analysis and parametric analysis of key input parameters. Several performance indicators were first defined and then used to compare the performance of both heat pump systems.

The flow chart of the modeling methodology for two-stage ACHP in this master thesis is shown in figure 3.1.

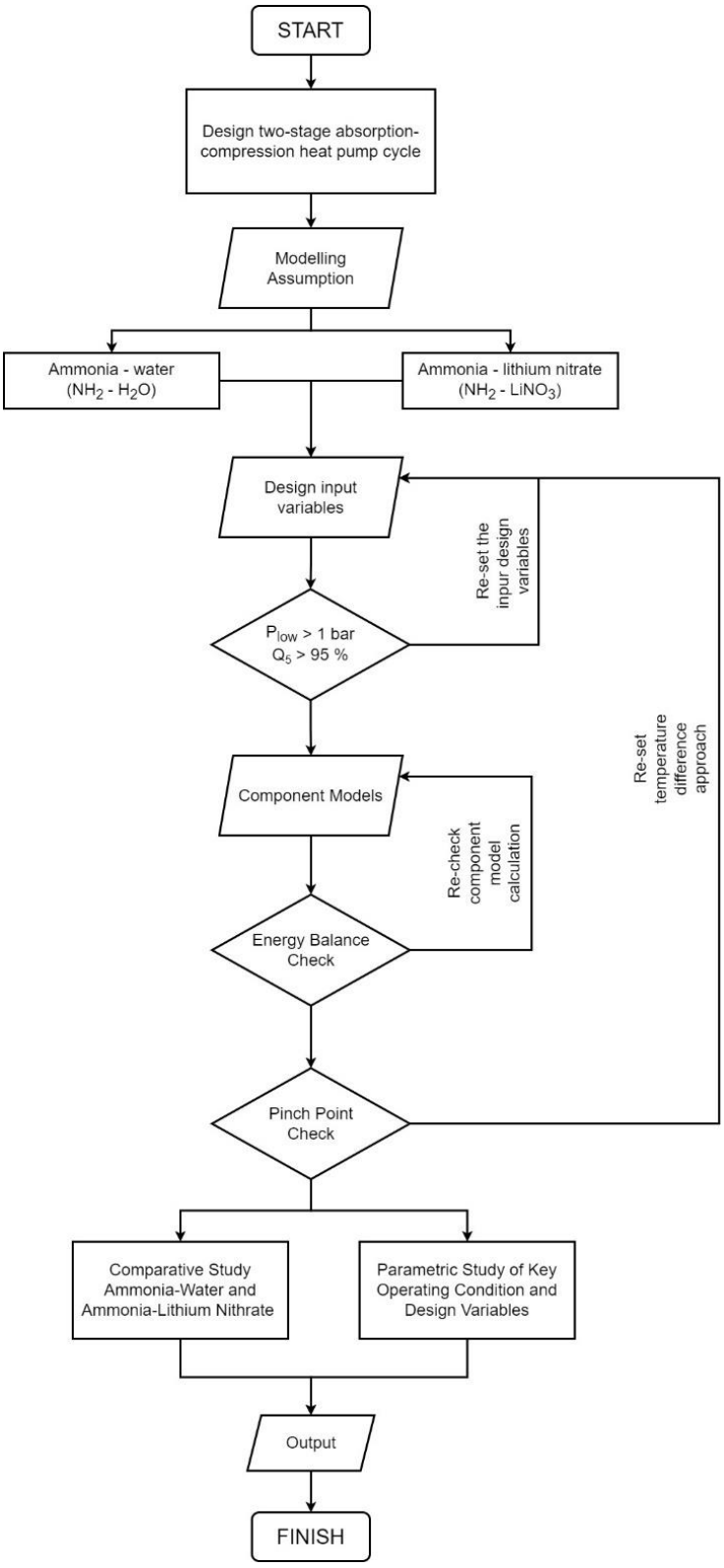

Figure 3.1. Flow chart diagram of the modeling methodology

The ACHP system started by modeling the two-stage absorption-compression heat pump cycle that is compatible with zeotropic mixtures and supplies heating and cooling applications at the

same time. The next step is to set up both modeling assumptions, input parameters, and the properties of the mixtures and the heat transfer fluid for the heating supply and cooling supply that want to be used in the system. Afterward, the energy and mass balance of each component is applied.

3.2 Modelling Assumptions

The following presumptions were made to develop the double-stage ACHP using ammonia-water and ammonia-$LiNO_3$ mixtures:

- The system is working under steady-state conditions.
- Heat losses and pressure drops in heat exchangers and connecting pipes are neglected.
- The weak solution that exits from the desorber (state 6) is in equilibrium with the vapor that leaves the desorber (state 5).
- The vapor (state 5) and liquid solution (state 6) leaving the desorber are saturated at the corresponding temperature and pressure.
- The ammonia-water/ammonia-lithium nitrate solution, strong in ammonia, at the exit of the absorber is saturated (state 1).
- The mixing process at the absorber is adiabatic.
- The process in the expansion valve is isenthalpic.

3.3 Component Models

The component models are developed to calculate every single process that happens in the ACHP system. The equations are based on mass and energy balance equations according to the second law of thermodynamics in each component. Considering the assumptions considered above, the mass and energy balances of each component are expressed as follows:

Overall mass balance:

$$\sum \dot{m}_{in} = \sum \dot{m}_{out}\,, \tag{3.1}$$

Where $\dot{m}_{in}$ is the mass flow at the inlet stream and $\dot{m}_{out}$ is the mass flow rate at the outlet stream.

Component mass balance:

$$\sum \dot{m}_{in} \cdot z_{in} = \sum \dot{m}_{out} \cdot z_{out} \tag{3.2}$$

where z_{in} is the ammonia mass fraction at the inlet stream and z_{out} is the ammonia mass fraction at the outlet stream.

$$\sum \dot{m}_{in} \cdot h_{in} + \sum \dot{Q}_{in} = \sum \dot{m}_{out} \cdot h_{out} + \sum \dot{Q}_{out} \tag{3.3}$$

where h_{in} is the specific enthalpy of the inlet stream, h_{out} is the specific enthalpy of the outlet stream, $\dot{W}$ and $\dot{Q}$ are the heat flow and workflow rates.

For the compressor modeling, the first step is to determine the outlet condition after the compression process, the value of the isentropic efficiency is used from equation 3.4.

$$h_{com,out} = h_{com,in} + \frac{h_{com,out,isen} - h_{com,in}}{\eta_{isen,com}} \tag{3.4}$$

where $h_{com,in}$ and $h_{com,out}$ are the specific enthalpy at the compressor inlet and outlet condition in kJ/kg respectively, $h_{com,out,isen}$ is the ideal specific enthalpy of the isentropic compression in kJ/kg, η_{isen} is the isentropic efficiency.

After collecting data from the several papers that showed in table 2.2, this ACHP system was calculated with equation 3.5 which is obtained by the collected data from the manufacturers for the isentropic efficiency of the compressor which has the higher temperature discharge (Wersland *et al*, 2018) which is obtained using equation 3.5.

$$\eta_{isen,com} = 0.7876 - 0.0006 pr_{com} \tag{3.5}$$

Equation 3.6 is applicable for piston compressors and it is dependent on the pr_{com} or pressure ratio of the compressor. The pr_{com} is defined in equation 3.6.

$$pr_{com} = \frac{P_{com,out}}{P_{com,in}} \tag{3.6}$$

where $P_{com,in}$ and $P_{com,out}$ are the pressure at the inlet and outlet of the compressor in bar.

The ACHP system is working with pressure levels, which are high pressure (P_{high}), low pressure (P_{low}), and intermediate pressure (P_{mid}). The value of the intermediate pressure can be obtained using equation 3.7.

$$P_{mid} = \sqrt{\left(\frac{T_H}{T_L}\right) P_{low} \cdot P_{high}} \tag{3.7}$$

where T_H is the condenser (or absorber) temperature (K) and T_L is the evaporator (or desorber) temperature (K). The P_{mid} significantly influences the performance of the heat pump and is calculated using equation 3.7. It is possible to estimate the P_{mid} closer to the ideal intermediate pressure of real two-stage ACHP systems without optimization instead of using the geometric mean of the low and high system pressures throughout the simulation.

The electrical power consumption of the compressor can be calculated by equation 3.8.

$$\dot{W}_{com,el} = \frac{\dot{m}_{com}\,(\,h_{com,out} - \,h_{com,in})}{\eta_m} \tag{3.8}$$

where in this case, the losses through the mechanical transmission components in the compressor are neglected. $\dot{W}_{com,el}$ is the electrical power consumption of the compressor in kW and η_m is the efficiency of the electric motor (95 %).

While using the $\eta_{isen,com}$, the equation for the volumetric efficiency of the compressor, λ_{com}, for the piston compressor also obtained from (Wersland *et al*, 2019):

$$\lambda_{com} = \,1.0056 - 0.0374 pr_{com} \tag{3.9}$$

The stoke volumes of the compressors are calculated by equation 3.10.

$$\dot{V}_{com} = \frac{\dot{m}_{com} v_{com,in}}{\lambda_{com}} \tag{3.10}$$

where $v_{com,in}$ is the suction line-specific volume in m^3/kg.

The solution pump power consumption can be obtained by equation 3.11.

$$\dot{W}_{sp} = (P_{sp,out} - P_{sp,in})\,\frac{v_{sp,in} \cdot \dot{m}_{sp}}{\eta_{sp}} \tag{3.11}$$

where $P_{sp,in}$ and $P_{sp,in}$ are the pressure before and after leaving the pump in kPa, $v_{sp,in}$ is pump suction line specific volume in m^3/kg and η_{sp} is pump efficiency which a value is 75 % (Jensen *et al.*, 2015). After knowing the value of work at the pump, the solution pump's electrical power consumption also can be calculated by equation 3.12.

$$\dot{W}_{sp,el} = \frac{\dot{W}_{sp}}{\eta_m} \tag{3.12}$$

where η_m is electrical motor efficiency driving the pump (95 %).

The heat duty of the absorber and the desorber can be defined by the energy balance around the absorber and the desorber, respectively, considering the streams entering and leaving the component by referring only to the heat exchanging part of the absorber and the desorber.

The heat capacitance can be calculated by equation 3.13 below.

$$\dot{C} = (\dot{m}C_p) \tag{3.13}$$

where C_p is specific heat capacity in kJ/kg-K, $\dot{C}$ is heat capacitance in kW/K and $\dot{m}$ is mass flow while passing the heat exchanger. The minimum of the heat capacitance obtained from both the cold and hot sides is used to calculate the heat duty of the heat exchanger as calculated below.

$$\dot{Q}_{shx} = \varepsilon \cdot \dot{C}_{min} \cdot (T_{h,in} - T_{c,in}) \tag{3.14}$$

$\dot{Q}_{shx}$ is heat duty of heat exchanger in kW, $\dot{C}_{min}$ is minimum thermal capacitance in kW/K, ε is heat exchanger effectiveness in % and, $T_{h,in}$ and $T_{c,in}$ are inlet temperatures of both the hot and cold streams, respectively.

The vapor-liquid heat exchanger (VSHX) is used to cool the vapor before entering the compressor (state 9) by using the weak solution (stream 8 → 10), thereby, the temperature at the exhaust of the high-stage compressor is reduced. The maximum value of the effectiveness is set to make sure while the heat exchanging process the outlet of the vapor stream leaving VSHX still in saturated vapor condition ($Q_9 = 1$).

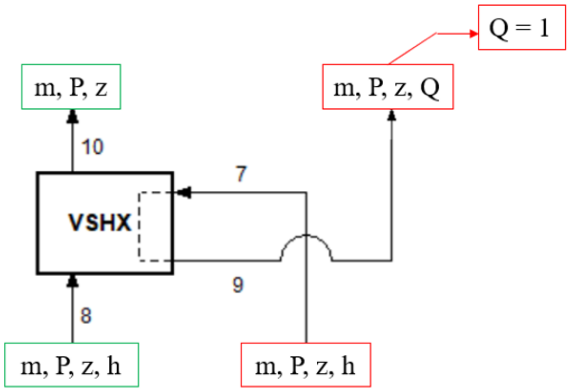

Figure 3.2. Schematic of the heat exchanging process for the vapor-solution heat exchanger.

While assuming state 9 is saturated vapor, and calling the other properties by that condition, the $\dot{Q}_{act}$ can be calculated with equations 3.15 and 3.16.

$$\dot{Q}_{act} = \dot{Q}_{vshx-c} = \dot{Q}_{vshx-h} \tag{3.15}$$

$$\dot{Q}_{vshx-h} = \dot{m}_7 h_7 - \dot{m}_9 h_9 \tag{3.16}$$

whereby equation 3.17, the enthalpy at state 10 (h_{10}) can be calculated also by equation 3.17.

$$\dot{Q}_{vshx-c} = \dot{m}_{10} h_{10} - \dot{m}_8 h_8 \tag{3.17}$$

The maximum possible heat transfer $\dot{Q}_{max}$ can also be calculated by equation 3.18.

$$\dot{Q}_{max} = \left(\dot{m}c_p\right)_{min} \Delta T_{in} \tag{3.18}$$

$$\dot{Q}_{max} = \left(\dot{m}c_p\right)_{min} (T_7 - T_8) \tag{3.19}$$

where $\left(\dot{m}c_p\right)_{min}$ obtained from the minimum thermal capacitance of both streams.

Then, by getting the value of $\dot{Q}_{max}$, the maximum VSHX effectiveness to prevent any liquid form before entering the second compressor can be calculated also by equation 3.20.

$$\varepsilon = \frac{\dot{Q}_{act}}{\dot{Q}_{max}} \tag{3.20}$$

3.4 Thermodynamic Properties

3.4.1 Ammonia-water mixture

The zeotropic mixture of ammonia-water properties is calculated by the procedure provided in EES at subcooled, saturated, and superheated conditions. Three out of the eight properties that can be obtained through the process must be provided for the zeotropic working fluid of ammonia water. With this procedure, all the properties of each state of the double-stage ACHP system can be calculated and the performance of the system can be analyzed as well.

An equation of state for ammonia-water mixtures provided by EES was obtained by the correlation of ammonia-water where the gas and liquid states are provided separately (Ibrahim and Klein, 1993). The gas phase was assumed as an ideal solution and the Gibbs excess energy was used to allow departure from the ideal solution behavior in a liquid phase. The correlation covers vapor-liquid equilibrium pressures of 0.2 to 110 bar and temperatures of 230 to 600 K.

3.4.2 Ammonia-Lithium Nitrate

The ammonia-lithium nitrate calculation to call the properties is not available on the EES, therefore, to calculate the ACHP with ammonia-lithium nitrate as a working fluid is by the correlation using the experimental data that has been investigated by the research group on applied thermal engineering (CREVER). Libotean *et al.* (2007, 2008) measured the properties

of ammonia + lithium nitrate (density, viscosity, and heat capacity) limited only in an ammonia mass fraction range from 0.35 to 0.65 and temperatures from 20 ˚C to 80 ˚C. For this reason, the recent study presents new correlations obtained based on the new experimental data of ammonia–lithium nitrate (from 0.2 to 0.65 in ammonia mass fraction and up to 150 ˚C (Salavera *et al*., 2018). Several states are not in saturated liquid condition (state 3, state 4, and state 13), in consequence, the vapor-liquid phase approach should be calculated to obtain the value of the properties.

3.4.2 Heat and cold transfer mediums

For the external circuit, two types of solutions are used on each stream. In the heat sink, the temperature will be above 90 ˚C, therefore, pressurized water is a good option to be selected to carry the heat sink's external stream. The pressure needs to be increased depending on the heating supply on the heat sink because if it is work above 100 ˚C and the pressure is still in the atmospheric pressure, the vapor will be generated in that stream. To prevent this situation happens, the pressure of the external heat sink should be increased to 2 bar. The property of water provides also by EES with the same properties as "Steam and Steam_IAPWS". The heat source works on the temperature below 0 ˚C below the freezing point of water, therefore, water is not eligible to be the cold carrier in the heat source. 30 % EG/water mixtures are used as an alternative to pure water for the external stream on the heat source. The properties of 30 % EG/water mixtures or also called brines are combinations of water plus an additional ingredient that lowers the freezing point of the fluid.

3.5 Energy Performance Indicators

The ACHP system is evaluated by several indicators to know how efficiently the performance of the system is carried out. Based on the first law and second law of thermodynamics which are equations to measure the energy efficiency of the ACHP system for further discussion in the next chapter (Cengel *et al*, 2015).

The combined COP of ACHP for simultaneous heating and cooling supply is defined by equation 3.39.

$$COP_{shc} = \frac{\dot{Q}_{abs} + \dot{Q}_{des}}{\dot{W}_{lcomp,el} + \dot{W}_{hcomp,el} + \dot{W}_{sp,el}} \tag{3.25}$$

where $\dot{Q}_{abs}$ and $\dot{Q}_{des}$ are for the heat duty of the heating and cooling supplies. $\dot{W}_{lcomp,el}$ and $\dot{W}_{hcomp,el}$ are power consumption of LCOM and HCOM and $\dot{W}_{pump,el}$ is the power consumption of the solution pump.

The volumetric capacity for simultaneous heating and cooling supply is calculated by equation 3.26.

$$VSCH = \frac{\dot{Q}_{abs} + \dot{Q}_{des}}{\dot{V}_{lcom} + \dot{V}_{hcom}} \tag{3.26}$$

where $\dot{V}_{lcom}$ and $\dot{V}_{hcom}$ are displacement volumes of the low compressor and high compressor that the value is already obtained using equation 3.12 and the $VSCH$ value is in kJ/m^3.

The ideal COP of simultaneous heating and cooling of the ACHP system can be obtained by the following equation 3.27.

$$COP_{ideal} = \frac{\bar{T}_{hw} + \bar{T}_{cf}}{\bar{T}_{hw} - \bar{T}_{cf}} \tag{3.27}$$

where $\bar{T}_{hw}$ and $\bar{T}_{cf}$ are the entropic average temperatures for the heat sink (pressurized hot water) in K and heat source (30 % EG/water mixtures) which those values can be obtained by equation 3.28.

$$\dot{T} = \frac{\Delta h}{\Delta s} \tag{3.28}$$

where Δh and Δs are the difference enthalpy and entropy of both the heat sink and heat source. The combined exergy COP is also used to calculate the exergy efficiency of the ACHP system, which can be obtained by the following equation 3.29.

$$ECOP_{shc} = \frac{\dot{Q}_{abs}\left(1 - \frac{T_{amb}}{\bar{T}_{hw}}\right) + \dot{Q}_{evap}\left(1 - \frac{T_{amb}}{\bar{T}_{cf}}\right)}{\dot{W}_{lcomp,el} + \dot{W}_{hcomp,el} + \dot{W}_{pump,el}} \tag{3.29}$$

where T_{amb} is the ambient temperature which the value settled as 288 K (15 ˚C).

The second-law efficiency of the ACHP system, $\eta_{II,shc}$, is defined by equation 3.30.

$$\eta_{II,shc} = \frac{COP_{shc}}{COP_{ideal,shc}} \tag{3.30}$$

3.6 Input Modelling Parameters

Table 3.1. Input modeling parameters for performance simulation of the double-stage absorption-compression system (Figure 2.1)

Parameters	**State**	**Unit**	**Value**
Operating Conditions			
(Base Case)			
Heat sink supply temperature	T_{17}	˚C	90
Heat source supply temperature	T_{15}	˚C	0
(Parametric Case)			
Heat sink supply temperature	T_{17}	˚C	90 – 105
Heat source supply temperature	T_{15}	˚C	-10 – 10
Design Variables			
Mass flow strong solution	$\dot{m}_1$	kg/s	1
High Pressure	P_{high}	Bar	25/30
Leaving absorber temperature	T_1	˚C	90
Leaving absorber temperature	T_4	˚C	0
Absorber cold end terminal temperature difference	$\Delta T_{abs,c}$	˚C	15
Desorber hot end terminal temperature difference	$\Delta T_{des,h}$	˚C	10
Strong solution and weak solution mass fraction difference	Δz	%	0.05/0.06
Heat sink temperature glide	$T_{hw,glide}$	K	15
Heat source temperature glide	$T_{cf,glide}$	K	6
SHX effectiveness	ε_{shx}	%	85
Pump efficiency	η_{sp}	%	75

4 SIMULATION RESULTS AND DISCUSSION

The schematic of the absorption-compression heat pump is simulated by two types of mixtures which are ammonia-water and ammonia-lithium nitrate. This section discussed the comparison of the performance of those two mixtures in the same schematic diagram and the same limitation of heat pump technologies. Two types of methods will be presented in this chapter to compare the two different mixtures, the first one is base case analysis and then the second one is the parametric study.

The limitation of the compressor temperature discharge has been already discussed and shown in chapter 2 and chapter 3 which the maximum temperature allowed by the compressor technologies for the ammonia is limited up to 190 ˚C (T_7 and T_{11} $\leq$ 190 ℃) (Bamigbetan *et al.*, 2017). The water content for the compressed vapor also settled at a certain condition that must be lower than 5% ($z_5 \geq 0.95$) (Jensen *et al.*, 2015) . Additionally, the sub-atmospheric pressure operating conditions of the heat must be avoided of $P_{low} > 1.0\ bar$ to prevent the ambient air from entering the system and eliminate the entrainment of air in the system (Jensen *et al.*, 2015).

4.1 Base Case Analysis

In the base case analysis, the main purpose is to compare the performance of ammonia-water and ammonia-lithium nitrate. Based on first-law and second-law thermodynamics, four performance indicators are set to compare these two mixtures. Each system is evaluated with the same design variables and operating conditions. In base case analysis it will be presented the data of the simulation for two mixtures in each state to evaluate thermodynamically. The heat pump in this case is evaluated for the temperature supply for heating at 90 ˚C and temperature supply for cooling at 0 ˚C. Both systems work in the same design variables which are given in table 3.1. The high pressure is settled with the same value of 30 bar. The systems both work also in the same temperature at leaving absorber and desorber. By assuming a saturated condition, the mass fraction can be obtained to calculate the low pressure of the system with the input of Δz = 0.05 and assuming the saturated liquid condition. The absorber and the desorber minimum temperature difference are selected as well ($\Delta T_{abs,c}$ = 15 ˚C and $\Delta T_{des,h}$ = 10 ˚C) by the consideration of the pinch point of the system controlled above 3 ˚C. For the external circulation, the temperature glide of both external streams is fixed as input regarding the industrial need for simultaneous heating and cooling applications

($\Delta T_{hw,glide} = 15$ K and $\Delta T_{cf,glide} = 6$ K). The efficiency of the component and effectiveness of the heat exchanger are also given in table 3.1 as input respectively. With all those inputs and assumptions, the ammonia-water system and the ammonia-lithium nitrate system can be calculated and simulated by the engineering equation solver (EES). Detailed results for the thermodynamic state of points for both mixtures are provided in Table 4.1 And Table 4.2.

Table 4.1. Thermodynamic parameters of key points for ammonia-water.

State point	T (°C)	P (bar)	z (kg/kg)	ṁ (kg/h)	Q (kg/kg)	h (kJ/kg)	s (kJ/kg-K)
1	90.00	30	0.6506	1	0	211.16	1.17
2	28.82	30	0.6506	1	sc	-79.80	0.29
3	-4.68	1.647	0.6506	1	0.111	-79.80	0.34
4	-4.00	1.647	0.6506	1	0.125	-56.18	0.43
5	-4.00	1.647	0.9997	0.1253	1	1283.50	5.14
6	-4.00	1.647	0.6006	0.8747	0.000	-248.07	-0.25
7	140.38	7.977	0.9997	0.1253	sh	1592.87	5.30
8	-3.64	30	0.6006	0.8747	sc	-243.39	-0.24
9	26.32	7.977	0.9997	0.1253	1	1308.23	4.50
10	5.23	30	0.6006	0.8747	sc	-202.62	-0.09
11	150.95	30	0.9997	0.1253	sh	1567.65	4.63
12	77.28	30	0.6006	0.8747	sc	130.02	0.97
13	93.78	30	0.6506	1	0.078	310.13	1.44
14	6.00	1.013	-	1.074	-	226.68	1.10
15	0.00	1.013	-	1.074	-	200.00	1.00
16	75.00	2	-	1.572	-	314.16	1.02
17	90.00	2	-	1.572	-	377.14	1.19

sh = superheated
sc = subcooled

As shown in table 4.1 and table 4.2 are the values of properties in each state. Start from state 1 until state 13 are internal systems and 14-15 and 16-17 are the external systems for the cooling supply (desorber) and heating supply (absorber). The calculation process is the same for both ammonia-water and ammonia lithium nitrate, the huge difference is shown in state 5 of the system. In the ammonia-water mixture, while the separation process of the liquid and the vapor, there is a tiny amount of the vapor water that enters the compressor stream (state 5 → state 7 and state 9 → state 11) and creates an impact that the mass fraction at the stream is not precisely single liquid ($z_5 = 0.9997$), nevertheless, it's still tolerable because the compressor still can accept the amount of water as long as the value is lower than 5 % ($z \geq 0.95$) (Jensen *et al.*, 2015). For the ammonia-lithium nitrate mixture, this problem is not an issue that should be considered because the high boiling temperature of ammonia-lithium nitrate is high and cannot generate the vapor fraction of the lithium nitrate that could be entered the compressor stream.

Table 4.2. Thermodynamic parameters of key points for ammonia-lithium nitrate.

State point	T (˚C)	P (bar)	z (kg/kg)	ṁ (kg/h)	Q (kg/kg)	h (kJ/kg)	s (kJ/kg-K)
1	90.00	30	0.5844	1	0	290.25	-
2	33.27	30	0.5844	1	sc	95.00	-
3	-5.94	1.095	0.5844	1	0.089	95.00	-
4	-4.00	1.095	0.5844	1	0.107	129.73	-
5	-4.00	1.095	1	0.1074	1	1457.77	6.34
6	-4.00	1.095	0.5344	0.8926	0	-25.57	-
7	165.96	6.505	1	0.1074	sh	1851.88	-
8	-2.81	30	0.5344	0.8926	sc	-21.81	-
9	11.62	6.505	1	0.1074	1	1473.49	5.47
10	11.57	30	0.5344	0.8926	sc	23.71	-
11	152.05	30	1	0.1074	sh	1765.91	-
12	78.24	30	0.5344	0.8926	sc	242.46	-
13	97.69	30	0.5844	1	0.082	406.05	-
14	6.00	1.013	-	1.76	-	226.68	1.10
15	0.00	1.013	-	1.76	-	200.00	1.00
16	75.00	2	-	1.839	-	314.16	1.02
17	90.00	2	-	1.839	-	377.14	1.19

sh = superheated
sc = subcooled

In consequence, the temperature for the pure ammonia vapor is higher than the ammonia-water vapor as appeared in table 4.1 and table 4.2 at state 7 which are 140.38 ˚C and 165.96 ˚C, repectively. The high outlet temperature of the LCOM impacted the maximum heat exchanger effectiveness of the ammonia-lithium nitrate cycle is higher than the ammonia-water cycle. As appeared in Tables 4.1 and 4.2, state 9 of the ammonia-lithium nitrate system has a lower temperature which is 11.57 ˚C than the ammonia-water system which reaches 26.32 ˚C. It has a lower temperature because it was corresponding to the saturated condition at state 9 and the enthalpy of the pure ammonia. The temperature drop between state 7 to state 9 is very high, which also impacts the effectiveness of VSHX that quite higher than the ammonia-water system. This condition at the same time also affects the temperature of leaving HCOM of the ammonia-lithium nitrate cycle a little bit higher that the other system and the enthalpy. For the ammonia-water system, the outlet HCOM is 150.95 ˚C, which is Where at the end of the cycle (state 13) the temperature is quite higher for the ammonia-lithium nitrate system creating the gap of the pinch point also higher. with the same design variables and the operating condition, the ammonia-lithium nitrate cycle potentially generates the higher temperature glide if the concern of the temperature difference in the pinch point must be higher than 3 ˚C ($T_{pp} \geq 3$ ˚C). The heat transfer process and the temperature difference are shown in figure 4.1.

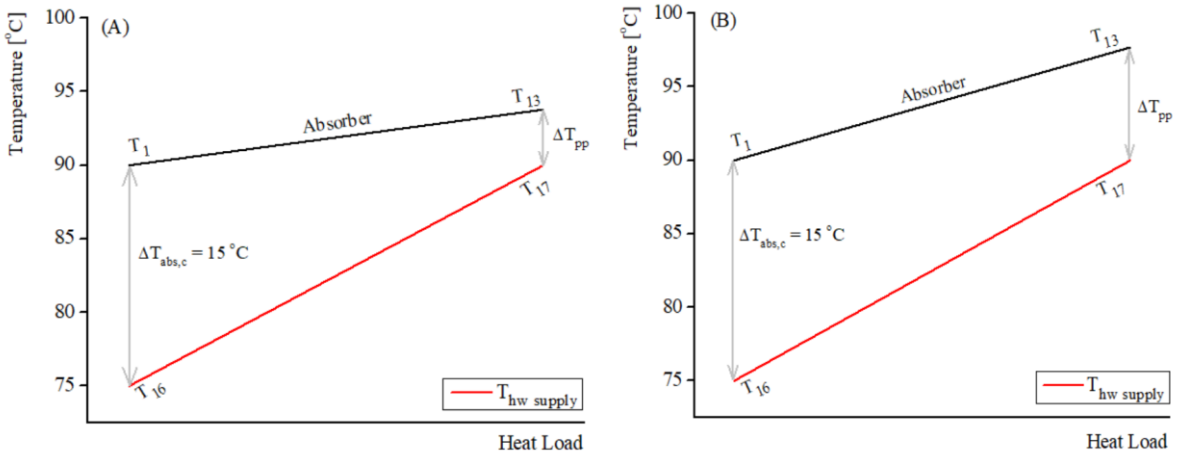

Figure 4.1. Heat transfer graph in the absorber (A) ammonia-water cycle, (B) ammonia-lithium nitrate cycle.

As shown in figure 4.1 (B), the temperature at state 13 is higher than the temperature at state 13 in figure 4.1 (A). The supply temperature of the ammonia-lithium nitrate can reach 97.69 ˚C which is 3.91 ˚C than the ammonia-water system that supplies the temperature at the inlet of the absorber is 93.78 ˚C. In consequence, because of the higher value of the pinch point in the ammonia-lithium nitrate system, the system has a lower area for transferring heat from the internal to the external and generates a lower cost production of the absorber system (reference). Supposing the area of the heat exchanger of both systems is the same, the ammonia lithium nitrate potentially produces the higher temperature glide of the external in the absorber because the value of the pinch point is quite high, and it can be increased until the near the maximum value that has been settled.

The same case also appears in the heat transfer at the desorber. The process described in figure 4.2 that shown above. While the heat transfer process from the external stream to the internal stream takes place, the ammonia-lithium nitrate system carries out with the lower temperature at the inlet of the desorber, which is -5.97 ˚C and for the ammonia-water is -4.68 ˚C. The gap of the pinch at the desorber for the ammonia-lithium nitrate is quite high and it potentially can be increased for the temperature glide to supply a lower temperature in the external stream lower than 0 ˚C. As well as has been discussed before, the readiness to reduce the manufacturing price is also substantial because of the decrement in the area because of the lower temperature that could be supplied.

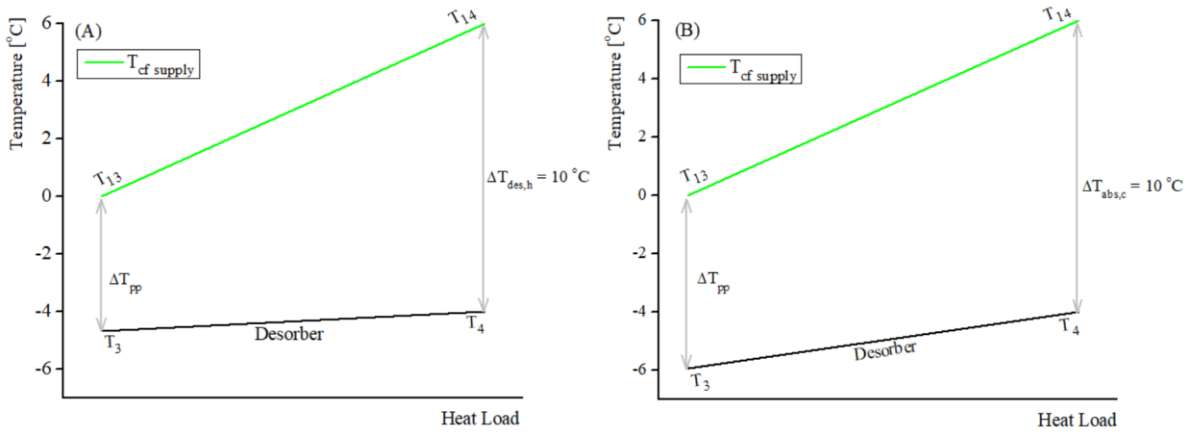

Figure 4.2. Heat transfer graph in the desorber (A) Ammonia-Water, (B) Ammonia-Lithium Nitrate.

For the mass flow at the external stream (state 14 → state 15 and state 16 → state 17), the ammonia-lithium nitrate also has a higher value which is 1.76 kg/s and 1.839 kg/s for the desorber and the desorber if we compare to the ammonia-water system that only has 1.074 kg/s for the desorber and 1.572 kg/s for the absorber. it indicates that the system of the ammonia-lithium water as the working fluid can generate an extraordinary hot supply and cold supply with the same design variables.

The detail of the working performances of both systems is compared and summarized in table 4.3 that shown below.

Table 4.3. Thermodynamic performances of the double-stage absorption-compression heat pump.

Items	**Units**	**Ammonia-water (NH_3-H_2O)**	**Ammonia-lithium nitrate (NH_3-$LiNO_3$)**
$\dot{Q}_{abs}$	kW	98.97	115.80
$\dot{Q}_{des}$	kW	23.62	38.72
$\dot{Q}_{shx}$	kW	290.0	195.3
$\dot{Q}_{vshx}$	kW	35.66	40.63
$\dot{W}_{sp}$	kW	4.10	3.35
$\dot{W}_{lcom}$	kW	38.76	42.32
$\dot{W}_{hcom}$	kW	35.50	31.40
COP_{shc}	-	1.554	1.913
$ECOP_{shc}$	-	0.2355	0.2631
$\eta_{II,shc}$	-	0.1954	0.2406
VSHC	kJ/m^3	863.0	867.9

Based on table 4.3, shows the performance of the system for the same operating conditions to supply heat at 90 ˚C and cold at 0 ˚C. As it has appeared above, the mass flow rate of the system (leaving absorber) for both systems is 1 kg/s, which for the absorber, the ammonia-lithium nitrate system provides 115 kW, and the ammonia-water system provides 98.97 kW. Regarding the desorber, both are supplied 38.72 kW and 23.62 kW. In addition, the total power input for the solution pump, the low compressor, and the high compressor for both systems are 78.36 kW and 77.07 kW. By the reason of the higher heat duty supplied to the external for the ammonia-lithium system and lower total power input as well, consequently, it has had a 23.10 % higher value of COP_{shc} and 11.71 % for $ECOP_{shc}$ as well. With the same value of COP ideal because of the same entropic average temperatures for chilled fluid and hot water, the ammonia-lithium nitrate system at the value of 0.2406 also has a 23.12 % higher value of the second-law efficiency ($\eta_{II,shc}$) than the ammonia-water, which is the amount that reaches 0.1954. Table 4.3 also shows that the value of VSCH between the two systems is quite close. The ammonia-water system reaches 863.0 kJ/m^3 and the ammonia-lithium nitrate reaches 876.9 kJ/m^3.

4.2 Parametric Study

In this section, the objective is to know the effect or influence of key operating conditions and design variables on system performances. By varying the input conditions, the exact parameters that highly influence the system can be known and then the best conditions that carried out the good output will be applied in the systems. The outputs of the external streams (T_{15} and T_{17}) are varied to get the operational conditions that can be used for the systems. The variation that can be used is only those values that are below the several limitations (compressor discharge temperature, low pressure, and water content) that have been discussed successively. Besides that, the values of the temperature pinch point in the absorber and the desorber are also maintained considerately ($T_{pp} \geq 3$ ℃). The analysis will focus on the comparison of the output of the parametric result between ammonia-water and ammonia-lithium nitrate. Several outputs will be compared to analyze the performance of those two systems with the varied output conditions for the heat supply temperature and the cold supply temperature. The heat duty of the absorber and desorber ($\dot{Q}_{abs}$ and $\dot{Q}_{abs}$), efficiency maximum of vapor-solution heat exchanger ($\varepsilon_{max,vshx}$), coefficient of performance (COP_{shc}), volumetric capacity (VSCH), exergy efficiency ($ECOP_{shc}$), and the second law of efficiency ($\eta_{II,shc}$) are the performance indicators to evaluate both systems at the operational condition for heating supply ($T_{hw} =$

$90 - 105$ ℃) and cooling supply ($T_{cf} = -0 - 10$ ℃). The simulation has been done by four conditions with the input of different mass fractions and high pressure. Simulation 1 calculated by Δz = 5% and $P_{high} = 30\ bar$, and simulation 2 also calculated with the same Δz but the high pressure is lower than simulation 1, which is $P_{high} = 25\ bar$. For simulations 3 and 4, the $P_{high} = 30\ bar$ and $P_{high} = 25\ bar$ but the Δz was increased to 6% to know the trend and the impact of the different mass fractions. The ammonia-water system and the ammonia-lithium nitrate system was analyzed by different simulation and the best condition with the high range of the operational condition was taken be created as a graph to analyze and compared the performance of both systems. Both are evaluated to supply the temperature starting from 90 ℃ until 105 ℃ and supplying cooling temperature from -10 ˚C until 10 ℃ at the same time. The data of the simulations are presented in table 4.4 and table 4.5 which appeared below.

Table 4.4. Simulation result for ammonia-water.

T_{15}	T_{17}	COP_{shc}	$ECOP_{shc}$	$\varepsilon_{max,VSHX}$	$\eta_{II,shc}$	$\dot{Q}_{abs}$	$\dot{Q}_{des}$	VSHC
Simulation 1 ($\Delta z = 5\ \%\ and\ P_{high} = 30\ bar$)								
-10	90	1.195	0.2031	0.8021	0.1719	97.45	10.92	496.6
-5	90	1.363	0.2168	0.7973	0.1837	98.09	17.29	660.5
0	90	1.554	0.2355	0.792	0.1954	98.97	23.62	863
5	90	1.768	0.2597	0.7869	0.2067	100	29.85	1108
10	90	2.009	0.2903	0.782	0.2175	101.2	35.95	1402
-5	95	1.078	0.2099	0.8054	0.1527	84.99	5.157	463.1
0	95	1.246	0.2249	0.8003	0.1653	86.01	11.36	621
5	95	1.435	0.245	0.7953	0.1777	87.16	17.49	816.3
10	95	1.647	0.271	0.7903	0.1896	88.47	23.51	1054
0	100	0.9835	0.2144	0.8065	0.1371	75.86	1.097	436.2
5	100	1.151	0.231	0.8014	0.1503	77.13	7.138	589.4
10	100	1.339	0.2529	0.7964	0.1632	78.53	13.09	779.4
10	105	1.072	0.2356	0.801	0.1378	70.31	4.005	563.7
Simulation 2 ($\Delta z = 5\ \%\ and\ P_{high} = 25\ bar$)								
0	90	1.451	0.2278	0.8057	0.1826	87.29	18.01	614.9
5	90	1.666	0.251	0.8006	0.1948	88.55	24.01	805.8
10	90	1.908	0.2808	0.7956	0.2065	89.95	29.91	1038

5	95	1.376	0.2398	0.8056	0.1704	79.83	14.41	597.7
10	95	1.59	0.2654	0.8005	0.1831	81.3	20.27	785.5
5	100	1.123	0.2284	0.8095	0.1467	72.46	5.871	434.8
10	100	1.314	0.2504	0.8043	0.1602	73.98	11.7	585
10	105	1.07	0.2355	0.8075	0.1377	67.59	3.842	426.4
Simulation 3 ($\Delta z = 6$ % $and\ P_{high} = 30\ bar$)								
-10	90	1.451	0.2175	0.8048	0.2088	129.1	26.7	578.4
-5	90	1.626	0.2343	0.7993	0.2191	129.3	33.68	757.8
0	90	1.82	0.256	0.7942	0.2289	129.6	40.47	974.9
5	90	2.038	0.2831	0.7893	0.2383	130.1	47.14	1235
10	90	2.283	0.3167	0.7844	0.2471	130.8	53.67	1542
-5	95	1.361	0.2304	0.8074	0.1927	115	20.21	558.7
0	95	1.534	0.2487	0.8023	0.2035	115.5	26.9	732.8
5	95	1.727	0.2721	0.7972	0.2138	116.2	33.47	944.2
10	95	1.943	0.3013	0.7922	0.2237	117.1	39.9	1198
0	100	1.29	0.2415	0.8081	0.1798	104.6	15.62	545.2
5	100	1.462	0.2616	0.803	0.1909	105.4	22.12	715.8
10	100	1.654	0.2869	0.798	0.2017	106.4	28.5	923.3
5	105	1.231	0.2512	0.8075	0.169	96.6	12.23	536.1
10	105	1.404	0.2732	0.8024	0.1805	97.66	18.57	704.4
10	110	1.183	0.2599	0.8059	0.16	90.23	9.649	530.2
Simulation 4 ($\Delta z = 6$ % $and\ P_{high} = 25\ bar$)								
0	90	1.736	0.2497	0.8074	0.2184	116.4	33.86	704.1
5	90	1.954	0.276	0.8022	0.2285	117.3	40.31	907.4
10	90	2.198	0.3088	0.7972	0.2379	118.3	46.65	1151
5	95	1.681	0.2681	0.8069	0.2082	108	29.79	697.6
10	95	1.899	0.2969	0.8018	0.2186	109	36.08	898.5
10	100	1.638	0.2853	0.8055	0.1997	101.3	26.72	695.2
10	105	1.408	0.2738	0.8085	0.1811	94.62	18.19	532.2

As the data that appears above, those are the operational condition of the double-stage absorption-compression heat pump to supply heating and cooling at the same time. The temperature at the outlet heat sink (T_{17}) is varied from 90 – 105 ˚C and the outlet heat source (T_{15}) is also varied from -10 – 10 ˚C. There are several data of the operational condition that

was eliminated because not sufficient and went beyond the limitation that has been discussed before, therefore, the data above is the one that safely passes the limitation and condition.

Table 4.5. Simulation result for ammonia-water.

T_{15}	T_{17}	COP_{shc}	$ECOP_{shc}$	$\varepsilon_{max,VSHX}$	$\eta_{II,shc}$	$\dot{Q}_{abs}$	$\dot{Q}_{des}$	VSHC
Simulation 1 ($\Delta z = 5$ % and $P_{high} = 30$ bar)								
0	90	1.913	0.2631	0.9145	0.2406	115.80	38.72	827.9
5	90	2.092	0.2879	0.9208	0.2446	115.61	43.18	1065
10	90	2.289	0.3174	0.9282	0.2478	115.52	47.54	1352
5	95	1.935	0.2914	0.9461	0.2396	113.32	38.47	836.9
10	95	2.113	0.3186	0.9543	0.2433	113.21	42.77	1077
10	100	1.949	0.3186	0.974	0.2376	110.53	37.88	859.6
Simulation 2 ($\Delta z = 5$ % and $P_{high} = 25$ bar)								
10	90	2.352	0.3235	0.9884	0.2545	117.08	49.51	988.5
Simulation 3 ($\Delta z = 6$ % and $P_{high} = 30$ bar)								
5	90	2.254	0.3021	0.9317	0.2636	146.86	59.55	1070
10	90	2.448	0.3328	0.9395	0.265	146.24	64.25	1356
10	95	2.277	0.3355	0.9641	0.2622	144.00	59.00	1080
10	100	2.119	0.3370	0.9828	0.2583	141.27	53.58	862.9
Simulation 4 ($\Delta z = 6$ % and $P_{high} = 25$ bar)								
10	90	2.499	0.3378	0.9971	0.2705	148.04	66.29	975.2

The data from simulation 1 that using the difference mass fraction of 5% and the high pressure of 30 bar has more flexible and variation operational conditions to supply heating and cooling than the other simulation. Thereupon, that data has been taken to be a representative of the cooling and heating supply of the system and will be analyzed and compared furtherly between ammonia-water and ammonia-lithium nitrate.

Figure 4.3 is showing the effect of cooling and heating supply as a function of the chilled fluid outlet temperature at different hot water supply temperatures with the result of simulation 1.

Because of the higher outlet temperature of HCOM for ammonia-lithium nitrate, the operational data of that working fluid does not have more variation than the ammonia-water system to supply the higher temperature of the outlet heat sink. As has been explained before,

the compressor technology has a limit that only can work with 190 ˚C as its temperature discharge. Because the pure ammonia fluid in the ammonia-lithium nitrate system potentially increases the temperature higher than the ammonia-water, therefore, the chance of the operation condition being eliminated or in the other word cannot be used to supply the higher value of the temperature in the heat sink is increased as well. Moreover, simulation 1 of the ammonia-water system can supply a higher temperature that can reach 105 ˚C, which is 5 points higher than ammonia-lithium nitrate. Not only that, to supply the lower temperature at the outlet of the heat source, it will increase the possibility to get a higher temperature at the outlet of HCOM, it makes the ammonia-lithium nitrate system only can supply 0 ˚C as a maximum temperature at the outlet of the heat sink.

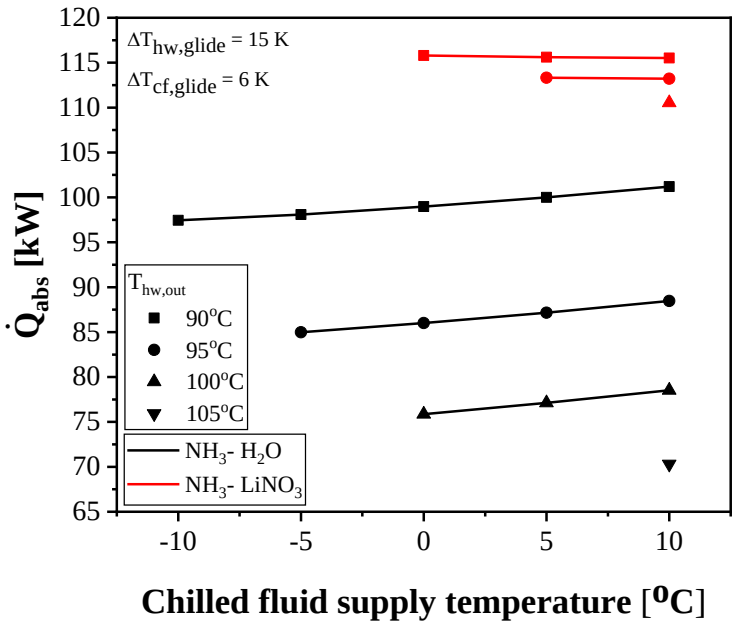

Figure 4.3 Effect of heating and cooling supply on heat duty of the absorber for ammonia-water and ammonia-lithium nitrate.

Figure 4.3 shows the effect of cooling and heating at the same time on the heat duty of the absorber. The ammonia-lithium nitrate even if the supply temperature is more limited than the ammonia-water system, can generate higher heat duty for the desorber. To generate the 90 ˚C heating supply and 0 – 10 ˚C cooling supply the heat duty average can reach 115.52 kW, which is higher than the ammonia-water system. For the other condition, if that is compared at the corresponding temperature of 95 ˚C and 100 ˚C, the ammonia-lithium nitrate also can supply the heat duty that the discrepancy is quite large compared to the ammonia-water. It can happen because the enthalpy of pure ammonia on the super-heated condition at the outlet of HCOM is

higher than the ammonia-water mixture, as a consequence of the higher enthalpy of the pure ammonia, the ammonia-lithium nitrate can generate a higher amount of heat duty in the absorber.

While supplying the cold temperature at 0 – 10 ˚C and hot temperature at 90 ˚C for the ammonia-lithium nitrate, the absorber produces the heat duties starting from 116.08 – 115.52 kW. For supplying a hot temperature of 95 ˚C, it generates the values from 113.21 – 113.32 kW and for a hot temperature is 100 ˚C, it supplies 110.53 kW. The ammonia-water system when supplying the cold temperature at -10 – 10 ˚C and the hot temperature at 90 ˚C, the heat duties range is 97.45 – 101.2 kW. When its 95 ˚C, the range is decreased and starts from 84.99 – 88.47 kW. For supplying 100 ˚C, the heat duty can generate from 77.13 – 78.53 kW, and for 105 ˚C can supply 70.31 kW.

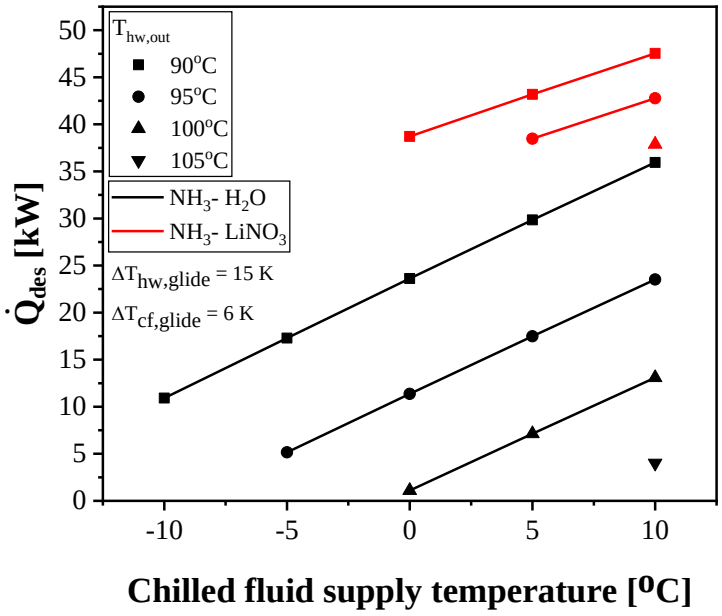

Figure 4.4. Effect of heating and cooling supply on heat duty of the desorber for ammonia-water and ammonia-lithium nitrate.

The same case also appears for the heat duty of the desorber. The lower enthalpy after leaving the expansion valve also triggers the higher high duty of the desorber. For supplying cold temperature at 0 – 10 ˚C and hot temperature at 90 ˚C, the heat duties at the desorber for each point are 38.72 kW, 43.18 kW, and 47.54 kW. While supplying heat at 95 ˚C, the heat duties decrease with the value of 38.47 kW and 42.77 kW, and for 100 ˚C because it only can supply the cold temperature at 10 ˚C, the value of heat duty is 37.88 kW. Then if compared to the ammonia-water system at the same value of operational condition for the ammonia-lithium

nitrate, the values are 23.62 kW, 28.85 kW, and 35.95 kW for supplying hot water at 90 ˚C, 28.85 kW, and 35 kW for supplying hot water at 95 ˚C and 13.09 kW for supplying hot water at 100 ˚C.

The maximum efficiency of the vapor-solution heat exchanger is calculated because of the highest limit of the effectiveness that saves to be used in the system. In the case of the system working as a function of the cold supply temperature at a different hot temperature supply is not allowed to pass the limit of the maximum effectiveness to maintain saturated vapor condition before entering the high compressor. State 9 is assumed at the saturated condition to obtain the value of maximum effectiveness in the VSHX.

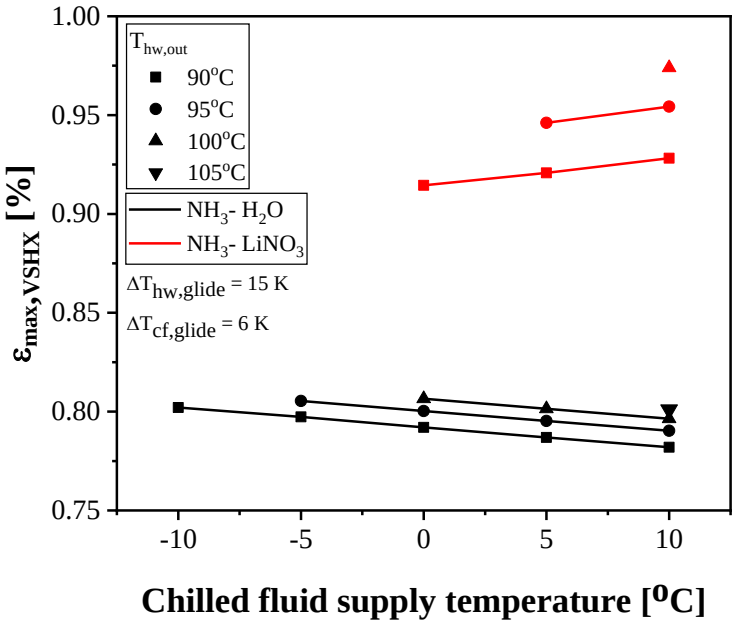

Figure 4.5. Effect of cooling and heating supply on maximum efficiency of the vapor-solution heat exchanger for ammonia-water and ammonia-lithium nitrate.

Table 4.5 shows the trend of maximum effectiveness with their different operational conditions. The higher heat sink supply temperature results in a higher value of the maximum VSHX effectiveness.

That figure also shows that the ammonia-lithium nitrate has a higher maximum effectiveness compared to the ammonia-water system. At its maximum, the effectiveness might reach up to 97 % for supplying 10 ˚C and 100 ˚C for cooling and heating. With the same supply temperature, the maximum effectiveness of ammonia only can reach 79 %. it can occur because

the temperature while leaving LCOM is quite high which can be reaching 180.71 ˚C and for ammonia-water is 150.62 ˚C.

As shown in figure 4.6, the higher temperature lift will decrease the value of COP_{shc}. It can happen because the compressor also works harder to elevate the temperature. For the ammonia lithium nitrate system, when the chilled fluid supply temperature increased from 0 ˚C to 10 ˚C, the lifted temperature will decrease, and the electrical power consumption of the heat pump ($\dot{W}_{lcomp,el} + \dot{W}_{hcomp,el} + \dot{W}_{pump,el}$) is also decreased by about 90.7-68.2 kW; 83.59-67.98 kW; 73.22-68.44 kW and 69.35 kW when the hot water supply temperature is 90 ˚C, 95 ˚C, 100 ˚C, and 105 ˚C. For the ammonia-lithium nitrate system, when the chilled fluid supply temperature increased from 0 ˚C to 10 ˚C it also decreased about 80.71-71.22 kW; 78.43-73.81 kW and 76.15 kW when the hot water supply temperature is 90 ˚C, 95 ˚C, and 100 ˚C.

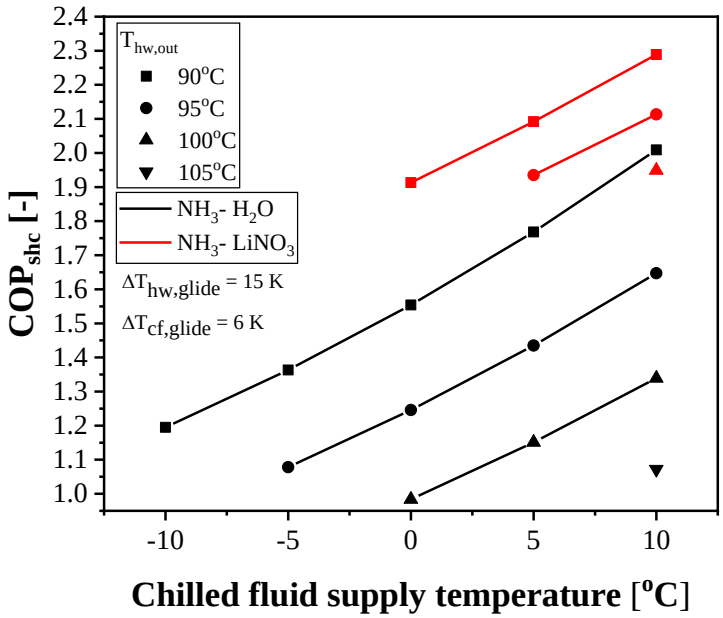

Figure 4.6. Effect of cooling and heating supply on combined COP (COP_{shc}) for Ammonia-Water and Ammonia-Lithium Nitrate.

Even the Ammonia-Lithium Nitrate has a higher value of electrical power consumption, it still has a higher value of combined COP (COP_{shc}) if compared with the ammonia-water system with the same supply temperature. It occurred because of the higher heat duties ($\dot{Q}_{abs} + \dot{Q}_{des}$) of the ammonia-lithium nitrate system that creates also a higher combined COP (COP_{shc}). The range value of COP_{shc} of the ammonia-lithium nitrate system to supply chilled fluid temperature from 0 - 10 ˚C and hot temperature from 90 – 100, ˚C is 1.913 to 2.289. for the

ammonia-water system, while supplying cold temperature at -10 to 10 ˚C and hot temperature at 90 to 105 ˚C, the range starts from 1.072 – 2.009.

Figure 4.7 shows the effect of the chilled fluid supply temperature on the second law efficiency ($\eta_{II,shc}$) of heat pump for simultaneous heating and cooling applications at the hot water supply temperature of 90 – 105 ˚C for the ammonia-water and 90 – 100 ˚C for ammonia-lithium nitrate.

The trend for both systems always increases following the increment of the chilled fluid supply temperature. The higher chilled fluid supply temperature will decrease the temperature lift and when the temperature lift is decreased at the same time will also increase the ideal COP. The value of ideal COP at the same cold and hot supplies for ammonia-water and ammonia-lithium nitrate is the same at the corresponding hot water and chilled fluid supply temperatures. The ideal COP of the corresponding reversible heat pump is decreased by about 6.95-9.24; 7.06-8.68; 7.17-8.20; 7.77 when the chilled fluid outlet temperature is raised from -10 ˚C to 10 ˚C for the hot water supply temperatures of 90 ˚C, 95 ˚C, 100 ˚C, and 105 ˚C, respectively. Synchronously the COP_{shc} of both systems will also increase as it is shown in figure 4.6. The $\eta_{II,shc}$ also will increase following the trend of both ideal COP and COP_{shc} when the chilled fluid supply temperature increases.

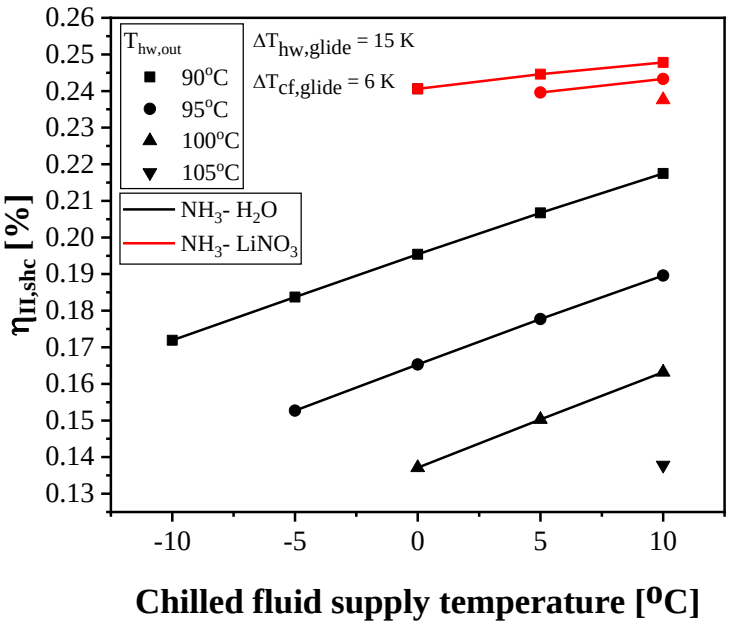

Figure 4.7. Effect of cooling and heating supply on second-law efficiency $\eta_{II,shc}$ for ammonia-water and ammonia-lithium nitrate.

Because the higher value of the COP_{shc} that has been discussed before in figure 4.6, creates a higher value of $\eta_{II,shc}$ for the ammonia lithium nitrate system than the ammonia-water as it appears in figure 4.7. For ammonia-water, the value of the $\eta_{II,shc}$ varied between 0.1371 and 0.2175 at the considered hot water temperature supply at 90 ˚C to 105 ˚C when chilled fluid supply temperature at -10 ˚C and increased until 10 ˚C. For ammonia-lithium nitrate, the value of the $\eta_{II,shc}$ varied between 0.2376 and 0.2478 at the considered hot water temperature supply at 90 ˚C to 100 ˚C when chilled fluid supply temperature at 0 ˚C and increased until 10 ˚C.

The exergy efficiency for simultaneous heating and cooling of both systems is shown in figure 4.8. The exergy efficiency of the ammonia-water varied between 0.2031 and 0.2903 for supplying hot temperature at 90 ˚C to 105 ˚C when chilled fluid supply temperature at -10 ˚C and increased until 10 ˚C. For the ammonia-lithium nitrate the value varied between 0.2631 and 0.3174 for supplying hot temperature at 90 ˚C to 105 ˚C when chilled fluid supply temperature at -10 ˚C and increased until 10 ˚C. The value of the $ECOP_{shc}$ decreases corresponding to the higher temperature supply at the heat sink. However, for the ammonia-lithium nitrate, there is an increment when supplying at the temperature of 95 ˚C.

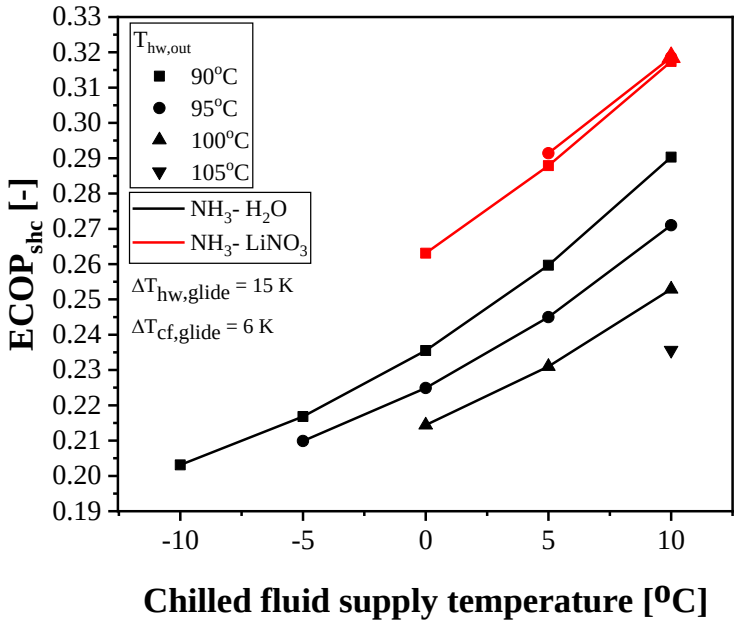

Figure 4.8. Effect of cooling and heating supply on exergy efficiency (ECOP_{shc}) for ammonia-water and ammonia-lithium nitrate.

The overall $ECOP_{shc}$ value of ammonia-lithium nitrate is higher than the ammonia-water system due to the higher heat duty of the ammonia lithium nitrate system that has been discussed before (see figure 4.3 and figure 4.4). The other factor is the electrical power

consumed by the heat pump which was involved also to calculate the $ECOP_{shc}$ that is defined in equation 3.43.

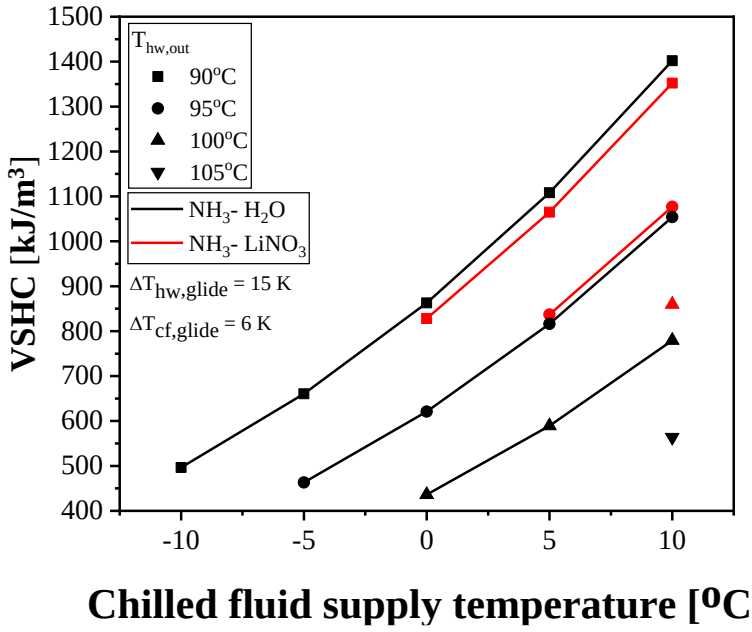

Figure 4.9. Effect of cooling and heating supply on VSHC for ammonia-water and ammonia-lithium nitrate.

The last comparison is VSHC shown in figure 4.9 below which is decreased by the corresponding hot water supply temperature of 90 ˚C, 95 ˚C, 100 ˚C and 105 ˚C for the ammonia-water system, respectively when the chilled fluid outlet temperature increased from -10 ˚C to 10 ˚C. For the ammonia-water system, the value of VSHC for heating supply at 90 ˚C, 95 ˚C, 100 ˚C, and 105 ˚C are 496.6 – 1402 kJ/m^3, 463.1 – 1054 kJ/m^3, 436.2 – 779.4 kJ/m^3, 413.7 – 563.7 kJ/m^3 and 563.7 kJ/m^3. For the ammonia-lithium nitrate system, the value of VSHC for heating supply at 90 ˚C, 95 ˚C, and 100 ˚C are 827.9 – 1352 kJ/m^3, 836.9 – 1077 kJ/m^3, and 859.6 kJ/m^3. The value of VSHC for both systems is quite similar because the accumulative value of the displacement volume of HCOM and LCOM for the ammonia-lithium nitrate is higher than the ammonia-water system caused by the suction line-specific volume.

As a result, the double-stage ACHP system using an ammonia-lithium nitrate mixture as a working fluid possesses several significant advantages over an ammonia-water mixture, including the ability to produce higher COP, ECOP, and second law efficiency with more or less the same value of VSHC. A high COP ensures a low operating cost and a high VSHC ensures a low investment cost, so the constraint on COP and VHSC ensures the economic viability of the heat pump (Jensen *et al.*, 2015).

5 CONCLUSIONS

A double-stage absorption-compression heat pump (ACHP) system was investigated for simultaneous heating and cooling supply for potential non-residential building and industrial applications using an ammonia-$LiNO_3$ mixture as a working fluid. Then, the energy and exergy performance of the ammonia-$LiNO_3$ ACHP system was compared to the ACHP system based on the conventional ammonia-water mixture under the same operating conditions.

In the base-case considered (i.e., hot water and chilled fluid supply temperatures of 90 °C and 0 °C, respectively, with heat sink and heat source temperature glides of 15 K and 6 K), the ammonia-$LiNO_3$ ACHP system produced 115 kW of heating and 38.7 kW of cooling outputs. While the ammonia-water ACHP system produced about 99 kW of heating and 23.6 kW of cooling outputs. The corresponding electrical power consumed by the ammonia-$LiNO_3$ and ammonia-water ACHP systems were 78.4 kW and 77.1 kW. Therefore, the combined COP (COP_{shc}) and exergy efficiency ($ECOP_{shc}$) of the ammonia-$LiNO_3$ ACHP system was higher than the ammonia-water ACHP system by about 23.1% and 11.7%, respectively. The second-law efficiency ($\eta_{II,shc}$) of the ammonia-$LiNO_3$ ACHP system is also higher by 23.1% of the ammonia-water ACHP system. The volumetric capacity for simultaneous heating and cooling (VSHC) delivery of the ACHP system was 867.9 kJ/m^3 for the case of the ammonia-$LiNO_3$ mixture and 863 kJ/m^3 for the ammonia-water mixture.

Finally, the performance of ammonia-$LiNO_3$ and ammonia-water ACHP systems were analysed for a range of hot water and chilled fluid supply temperatures of 90 °C to 105 °C and −10 °C to 10 °C, respectively. Under these conditions, the ammonia-water ACHP system operates at COP_{shc} of 1.072 to 2.009, $ECOP_{shc}$ of 0.203 to 0.29, $\eta_{II,shc}$ of 13.7 to 21.7%, and VSHC of 413.7 kJ/m^3 to 1402 kJ/m^3. On the other hand, the ammonia-$LiNO_3$ ACHP system operates at COP_{shc} of 1.913 to 2.289, $ECOP_{shc}$ of 0.263 to 0.317, $\eta_{II,shc}$ of 23.8% to 24.8%, and VSHC of 827.9 kJ/m^3 to 1352 kJ/m^3 when the hot water and chilled fluid are supplied in the range of 90 °C to 100 °C and 0 °C to 10 °C, respectively.

REFERENCES

Adamson, K.M. *et al.* (2022) 'High-temperature and transcritical heat pump cycles and advancements: A review', *Renewable and Sustainable Energy Reviews*. Elsevier Ltd. Available at: https://doi.org/10.1016/j.rser.2022.112798.

Agrawal, N. and Bhattacharyya, S. (2007) 'Studies on a two-stage transcritical carbon dioxide heat pump cycle with flash intercooling', *Applied Thermal Engineering*, 27(2–3), pp. 299–305. Available at: https://doi.org/10.1016/j.applthermaleng.2006.08.008.

Ahrens, M.U. *et al.* (2021) 'Integrated high temperature heat pumps and thermal storage tanks for combined heating and cooling in the industry', *Applied Thermal Engineering*, 189. Available at: https://doi.org/10.1016/j.applthermaleng.2021.116731.

Ahrens, M.U., Hafner, A. and Eikevik, T.M. (2019a) 'Compressors for ammonia-water hybrid absorbtion-compression heat pumps', *IRR Conference: Ammonia and CO2 Refrigeration Technologies*, 8.

Ahrens, M.U., Hafner, A. and Eikevik, T.M. (2019b) 'Development of ammonia-water hybrid absorption-compression heat pumps', in *Refrigeration Science and Technology*. International Institute of Refrigeration, pp. 4942–4949. Available at: https://doi.org/10.18462/iir.icr.2019.1869.

Ally, M.R., Sharma, V. and Abdelaziz, O. (2017) 'Exergy analysis of electrically- and thermally-driven engines to drive heat pumps: An exhaustive comparative study', *International Journal of Refrigeration*, 76, pp. 313–327. Available at: https://doi.org/10.1016/j.ijrefrig.2017.02.011.

Arpagaus, C. *et al.* (2018) 'High temperature heat pumps: Market overview, state of the art, research status, refrigerants, and application potentials', *Energy*. Elsevier Ltd, pp. 985–1010. Available at: https://doi.org/10.1016/j.energy.2018.03.166.

Ayou, D.S. and Coronas, A. (2022) 'Double-Lift Ammonia/Water Compression-Resorption Heat Pump for Simultaneous Industrial Process Heating and Refrigeration Applications', *Inernational Refrigeration and Air Conditioning Conference* [Preprint]. Available at: https://docs.lib.purdue.edu/iracc.

Ayou, D.S., Hargiyanto, R. and Coronas, A. (2022) 'Ammonia-based compression heat pumps for simultaneous heating and cooling applications in milk pasteurization processes:

Performance evaluation', *Applied Thermal Engineering*, 217. Available at: https://doi.org/10.1016/j.applthermaleng.2022.119168.

Bamigbetan, Opeyemi *et al.* (2017) 'EXTENDING AMMONIA HIGH TEMPERATURE HEAT PUMP USING BUTANE IN A CASCADE SYSTEM', *IRR Conference: Ammonia and CO2 Refrigeration Technologies* [Preprint]. Available at: https://www.researchgate.net/publication/318419589.

Bergland, M.G. (2011) *Optimizing the Compression/Absorption Heat Pump System at High Temperatures*. Norwegian University of Science and Technology.

Bjørvik, F. (2019) *Design of a hybrid absorption/compression high temperature heat pump test rig*. Norwegian University of Science and Technology.

Cengel, Y.A. and Boles, M.A. (2015) *Thermodynamics - An Engineering Approach*. 8th edn. New York: McGraw-Hill Education.

Chua, K.J., Chou, S.K. and Yang, W.M. (2010) 'Advances in heat pump systems: A review', *Applied Energy*. Elsevier Ltd, pp. 3611–3624. Available at: https://doi.org/10.1016/j.apenergy.2010.06.014.

Gao, P. *et al.* (2020) 'Hybrid absorption-compression heat pump with two-stage rectification and subcooler', *Applied Thermal Engineering*, 181. Available at: https://doi.org/10.1016/j.applthermaleng.2020.116027.

H Rlzvl, S.S. and Heldemann, R.A. (1987) 'Vapor-Liquid Equilibria in the Ammonia-Water System', *Journal of Chemical Enginering Data*, 32, pp. 183–191. Available at: https://pubs.acs.org/sharingguidelines.

Herold, K.E., Radermacher, R. and Klein, S.A. (2016) *ABSORPTION CHILLERS AND HEAT PUMPS*. 2nd edn. Boca Raton: Taylor & Francis Group.

Ibrahim, O.M. and Klein, S.A. (1993) 'Thermodynamic properties of ammonia-water mixtures', *ASHRAE Transactions: Symposia* [Preprint]. Available at: https://www.researchgate.net/publication/279905260.

International Energy Agency (2021) *Statistics report Key World Energy Statistics 2021*. Available at: https://www.iea.org/reports/key-world-energy-statistics-2021 (Accessed: 15 February 2023).

International Energy Agency (2022a) *Net Zero by 2050 - A Roadmap for the Global Energy Sector*. Available at: www.iea.org/t&c/.

International Energy Agency (2022b) *World Energy Outlook Special Report The Future of Heat Pumps*. Available at: www.iea.org.

Jensen, J.K. *et al.* (2014) 'Investigation of ammonia/water hybrid absorption/compression heat pumps for heat supply temperatures above 100 °C', *Proceedings of the International Sorption Heat Pump Conference*, 1, pp. 311–320.

Jensen, J.K. *et al.* (2015) 'On the development of high temperature ammonia-water hybrid absorption-compression heat pumps', *International Journal of Refrigeration*, 58, pp. 79–89. Available at: https://doi.org/10.1016/j.ijrefrig.2015.06.006.

Jung, C.W., An, S.S. and Kang, Y.T. (2014) 'Thermal performance estimation of ammonia-water plate bubble absorbers for compression/absorption hybrid heat pump application', *Energy*, 75, pp. 371–378. Available at: https://doi.org/10.1016/j.energy.2014.07.086.

Kim, J. *et al.* (2013) 'Experimental study of operating characteristics of compression/absorption high-temperature hybrid heat pump using waste heat', *Renewable Energy*, 54, pp. 13–19. Available at: https://doi.org/10.1016/j.renene.2012.09.032.

Kim, J.K., Son, H. and Yun, S. (2022) 'Heat integration of power-to-heat technologies: Case studies on heat recovery systems subject to electrified heating', *Journal of Cleaner Production*, 331. Available at: https://doi.org/10.1016/j.jclepro.2021.130002.

Kobe, K.A. and Emerson Lynn, R. (1952) *THE CRITICAL PROPERTIES OF ELEMENTS AND COMPOUNDS*. Available at: https://pubs.acs.org/sharingguidelines.

Libotean, S. *et al.* (2007) 'Vapor-liquid equilibrium of ammonia + lithium nitrate + water and ammonia + lithium nitrate solutions from (293.15 to 353.15) K', *Journal of Chemical and Engineering Data*, 52(3), pp. 1050–1055. Available at: https://doi.org/10.1021/je7000045.

Libotean, S. *et al.* (2008) 'Densities, viscosities, and heat capacities of ammonia + lithium nitrate and ammonia + lithium nitrate + water solutions between (293.15 and 353.15) K', *Journal of Chemical and Engineering Data*, 53(10), pp. 2383–2388. Available at: https://doi.org/10.1021/je8003035.

Liu, C. *et al.* (2018) 'A high-temperature hybrid absorption-compression heat pump for waste heat recovery', *Energy Conversion and Management*, 172, pp. 391–401. Available at: https://doi.org/10.1016/j.enconman.2018.07.027.

Liu, C. *et al.* (2019) 'Working domains of a hybrid absorption-compression heat pump for industrial applications', *Energy Conversion and Management*, 195, pp. 226–235. Available at: https://doi.org/10.1016/j.enconman.2019.05.013.

Markmann, B. *et al.* (2019) 'Experimental results of an absorption-compression heat pump using the working fluid ammonia/water for heat recovery in industrial processes', *International Journal of Refrigeration*, 99, pp. 59–68. Available at: https://doi.org/10.1016/j.ijrefrig.2018.10.010.

Neksfit, P. *et al.* (1998) 'CO2-heat pump water heater: characteristics, system design and experimental results*', *lnt J. Refrigeration*, 21(3), pp. 172–179.

Nordtvedt, S.R. (2005) *Experimental and theoretical study of a compression/absorption heat pump with ammonia/water as working fluid*. Norwegian University of Science and Technology.

Nordtvedt, S.R. *et al.* (2011) 'HYBRID HEAT PUMP FOR WASTE HEAT RECOVERY IN NORWEGIAN FOOD INDUSTRY', *International Heat Pump Conference*, 10. Available at: www.heatpumpcentre.org/en/hppactivities/ieaheatpumpconference.

Ommen, T., Markussen, W.B. and Elmegaard, B. (2014) 'Heat pumps in combined heat and power systems', *Energy*, 76, pp. 989–1000. Available at: https://doi.org/10.1016/j.energy.2014.09.016.

Qing, C., Gao, P. and Zhang, C.L. (2021) 'Thermodynamic analysis on feasible operating region of two-stage hybrid absorption-compression heat pump cycles', *International Journal of Refrigeration*, 121, pp. 43–50. Available at: https://doi.org/10.1016/j.ijrefrig.2020.09.017.

Richter, T.M.M. and Niewa, R. (2014) 'Chemistry of ammonothermal synthesis', *Inorganics*. MDPI Multidisciplinary Digital Publishing Institute, pp. 29–78. Available at: https://doi.org/10.3390/inorganics2010029.

Salavera, D. and Coronas, A. (2018) *Property Modeling of the Ammonia + Lithium Nitrate Mixture from New Experimental Data for Absorption Refrigeration Applications*.

Salehi, S. and Yari, M. (2019) 'Exergoeconomic assessment of two novel absorption-ejection heat pumps for the purposes of supermarkets simultaneous heating and refrigeration using NaSCN/NH3, LiNO3/NH3 and H2O/NH3 as working pairs', *International Journal of Refrigeration*, 101, pp. 178–195. Available at: https://doi.org/10.1016/j.ijrefrig.2019.03.029.

Wersland, M.B., Eikevik, T. and Tolstorebrov, I. (2018) 'Investigation of a hybrid compression absorption heat pump system for high temperatures', in *Refrigeration Science and Technology*. International Institute of Refrigeration, pp. 815–822. Available at: https://doi.org/10.18462/iir.gl.2018.1283.

Wersland, M.B., Kvalsvik, K.H. and Bantle, M. (2017) 'Off-design of high temperature hybrid heat pump', *IEA Heat Pump Conference*, 12.

Worrell, E. and Boyd, G. (2022) 'Bottom-up estimates of deep decarbonization of U.S. manufacturing in 2050', *Journal of Cleaner Production*, 330. Available at: https://doi.org/10.1016/j.jclepro.2021.129758.

Wu, W. *et al.* (2018a) 'A novel internally hybrid absorption-compression heat pump for performance improvement', *Energy Conversion and Management*, 168, pp. 237–251. Available at: https://doi.org/10.1016/j.enconman.2018.05.007.

Wu, W. *et al.* (2018b) 'A novel internally hybrid absorption-compression heat pump for performance improvement', *Energy Conversion and Management*, 168, pp. 237–251. Available at: https://doi.org/10.1016/j.enconman.2018.05.007.

Zhu, H. *et al.* (2022) 'Key technologies for smart energy systems: Recent developments, challenges, and research opportunities in the context of carbon neutrality', *Journal of Cleaner Production*. Elsevier Ltd. Available at: https://doi.org/10.1016/j.jclepro.2021.129809.

Zühlsdorf, B. *et al.* (2018) 'Improving the performance of booster heat pumps using zeotropic mixtures', *Energy*, 154, pp. 390–402. Available at: https://doi.org/10.1016/j.energy.2018.04.137.

UNIVERSITAT
ROVIRA i VIRGILI